

# X-RAY EMISSION FROM EXTRAGALACTIC JETS

D. E. HARRIS

*Harvard-Smithsonian Center for Astrophysics*

HENRIC KRAWCZYNSKI

*Washington University in St. Louis*

**Key Words** relativistic jets, X-ray jets, synchrotron emission, inverse Compton emission

**Abstract** This review focuses on the X-ray emission processes of extra-galactic jets on scales resolvable by the sub arcsec resolution of the Chandra X-ray Observatory. It is divided into 4 parts. The introductory chapter reviews the classical problems for jets, as well as those associated directly with the X-ray emission. Throughout this section, we deal with the dualisms of low powered radio sources versus high powered radio galaxies and quasars; synchrotron models versus inverse Compton models; and the distinction between the relativistic plasma responsible for the received radiation and the medium responsible for the transport of energy down the jet. The second part collects the observational and inferred parameters for the currently detected X-ray jets and attempts to put their relative sizes and luminosities in perspective. In part 3, we first give the relevant radio and optical jet characteristics, and then examine the details of the X-ray data and how they can be related to various jet attributes. The last section is devoted to a critique of the two non-thermal emission processes and to prospects for progress in our understanding of jets.

## TABLE OF CONTENTS

|  |    |
|--|----|
| THE PROBLEMS . . . . .   | 2  |
| <i>Jet Composition</i> . . . . .                               | 3  |
| <i>Jet formation, structure and propagation</i> . . . . .      | 4  |
| <i>Entrainment and Collimation</i> . . . . .                   | 7  |
| <i>Particle Acceleration and Emission Mechanisms</i> . . . . . | 8  |
| Physical Comparisons of Resolved X-ray Jets . . . . .          | 11 |
| <i>Gross jet properties</i> . . . . .                          | 11 |
| <i>Evaluation</i> . . . . .                                    | 12 |
| Observations of Resolved Jets . . . . .                        | 13 |
| <i>Relevant Radio and Optical Considerations</i> . . . . .     | 13 |

arXiv:astro-ph/0607228v1 11 Jul 2006

*The X-ray Data* . . . . . 15  
*Jet Detection Statistics* . . . . . 18

Discussion & Summary . . . . . 19  
*Critique of the Synchrotron Emission Model* . . . . . 19  
*Critique of the IC/CMB Emission Model* . . . . . 20  
*Tests to differentiate between synchrotron and IC/CMB models* . . . . . 22  
*Detectability of the Extended Jet Emission By Gamma-Ray Telescopes* . . . . . 23  
*Prospects* . . . . . 24  
*Summary* . . . . . 25

ACKNOWLEDGMENTS . . . . . 26

## 1 THE PROBLEMS

Jets are giant collimated plasma outflows associated with some types of Active Galactic Nuclei (AGN). The first jet was discovered in 1918 within the elliptical galaxy M87 in the Virgo cluster: “A curious straight ray lies in a gap in the nebulosity in p.a. 20°, apparently connected with the nucleus by a thin line of matter. The ray is brightest at its inner end, which is 11'' from the nucleus.” (Curtis 1918). At that time, the extended feature was a mere curiosity and its nature was not understood. When radio telescopes with good angular resolution and high sensitivities became available in the sixties, it was found that many galaxies exhibited extended radio emission consisting of a nuclear component, jets, hotspot complexes, and radio lobes. According to the standard picture, jets originate in the vicinity of a super-massive black hole (‘SMBH’ with several million to several billion solar masses) located at the center of the AGN; (c.f. the early ideas of Salpeter (1964)). The jets are most likely powered by these black holes, and the jets themselves transport energy, momentum, and angular momentum over vast distances (Blandford & Rees 1974, Rees 1971, Scheuer 1974), from the “tiny” black hole of radius  $r = 10^{-4} M_{\text{BH}}/10^9 M_{\odot}$  pc to radio hotspots, hotspot complexes and lobes which may be a Mpc or more away. Thus the study of jets must address a range of scales covering a factor of  $10^{10}$ !

Even now, after thirty years of intensive studies of radio galaxies in the radio regime, no consensus has emerged on their fundamental attributes such as composition, formation, and collimation. With the advent of the Hubble Space Telescope (HST) and the Chandra X-ray Observatory (CXO), the optical and X-ray emission from jets can be studied and new tests can be evaluated which were not possible based on radio data alone. This follows because the radio, optical, and X-ray jet emissions are emitted by electrons with quite different energies (i.e. Lorentz factors,  $\gamma$ ).

This review is focused on what X-ray observations of relativistic jets can contribute to our understanding of the physical processes in jets. Although some jet detections were made with the imaging X-ray observatories *Einstein* and *ROSAT*, significant progress blossomed only with the CXO (Weisskopf et al. 2003) launch in 1999. For this reason, together with the limitations of space, we emphasize results obtained between the years 2000 and 2005.5. We will concentrate on spatially resolved X-ray emission from the kpc-scale jets. Radio observations of the pc-scale jets and broadband observations of the spatially unresolved but highly variable core emission from the sub-pc jets of blazar-type AGN will only be discussed when they have direct implications for the inner workings of kpc-jets.

---

**CXO** Chandra X-ray Observatory: NASA’s first X-ray imaging satellite with sub-arc-second resolution. Launched in July 1999.

---

**Lorentz factor:** for relativistic electrons,  
 $\gamma = \frac{E}{m_e \times c^2}$ ; for the jet’s bulk velocity,  
 $\beta = \frac{v}{c}$ ,  $\Gamma = \frac{1}{\sqrt{1-\beta^2}}$ .

---

Furthermore, we will not cover Galactic X-ray jets even though they bear many similarities to their extragalactic counterparts. Although there have been reports of thermal X-ray emission associated with jets (mainly in the context of 'jet-cloud interactions'), our main concern is with the non-thermal emissions, already well established as the major process for radio through X-ray frequencies from multiple lines of argument including polarization data, Faraday screen parameters, X-ray spectral fitting, and the absence of emission lines.

Reviews on some aspects of jets include "Theory of extragalactic radio sources" (Begelman, Blandford & Rees 1984), "Beams and Jets in Astrophysics" (Hughes 1991), "Parsec-Scale Jets in Extragalactic Radio Sources" (Zensus 1997), and "Relativistic jets in AGNs" (Tavecchio 2004). Among the many jet related meetings in the last ten years are: "Relativistic jets in AGNs" Cracow, 1997, (Ostrowski et al. 1997); "Ringberg Workshop on Relativistic Jets" Ringberg Castle, 2001<sup>1</sup>; "The Physics of Relativistic Jets in the CHANDRA and XMM Era" Bologna, 2002, (Brunetti et al. 2003); "Triggering Relativistic Jets" Cozumel, 2005 (Lee & Ramirez-Ruiz 2006); and "Ultra-Relativistic Jets in Astrophysics: Observations, Theory and Simulations" Banff, 2005<sup>2</sup>. Conference reviews on the unresolved core emission have been given by Coppi (1999), Krawczynski (2004, 2005), Sikora & Madejski (2001) and Tavecchio (2005).

We use the conventional definition of spectral index,  $\alpha$ , for power-law radiation spectra: flux density,  $S_\nu \propto \nu^{-\alpha}$ . It is not yet known if electrons alone, or electrons and positrons radiate the observed jet emission. We thus refer in the following to either electrons or electrons and positrons as "electrons". We use  $\gamma$  as the Lorentz factor of particles in the jet-frame of reference, and  $\Gamma$  for the bulk Lorentz factor of the jet plasma. As most X-ray emitting jets are detected on only one side of otherwise double radio sources,  $\Gamma \geq$  a few seems likely to be generally applicable.

## 1.1 Jet Composition

We take the essence of a jet to be a quasi-lossless transmission line: a conduit containing relativistically moving particles and magnetic field (either of which could dominate the local energy) and/or Poynting flux. We distinguish between two substances: the "medium" which is responsible for delivering the power generated in the nucleus of the host galaxy to the end of the jet and thence to the radio lobes; and the non-thermal plasma responsible for the emission we detect in the radio, optical, and X-ray bands. While these two substances can be one and the same for some jet models, we prefer to think of them as quite distinct. Most models explain the appearance of radio, optical or X-ray bright hotspots in some jets as caused by the transfer of some form of energy (for example, energy associated with the medium's bulk motion or magnetic field energy), to highly relativistic emitting particles. The reader should note that we use the term "medium" lacking more precise knowledge about the nature of the jet material.

While the basic make-up of jets is still largely unknown, observations of polarized radio and optical emission show that at least some of the continuum jet emission originates as synchrotron emission from relativistic electrons gyrating in a magnetic field. Although we have this direct evidence about the emitting plasma, the jet medium responsible for delivering power to the end of the jets is

<sup>1</sup><http://www.mpa-garching.mpg.de/~enssln/Jets/Proceedings/>

<sup>2</sup>to download talks: <http://www.capca.ucalgary.ca/meetings/banff2005/index.html>

largely unconstrained. The jet medium cannot entirely consist of the relativistic electrons that produce the observed radiation since unavoidable inverse Compton (IC) losses off the cosmic microwave background (CMB) photons would preclude the flow of high energy electrons all the way to the end of some jets. Positing a minimal magnetic field strength of  $3\mu\text{G}$ , and ignoring the IC losses associated with starlight or quasar light which would shorten the relevant lifetimes even more, it has been shown that electrons with  $\gamma \geq$  a few thousand cannot survive for the time required to travel from the environs of the SMBH to the end of some jets (e.g. Harris & Krawczynski 2006).

The main contenders for the underlying jet medium are Poynting flux, electrons with  $\gamma \leq 1000$ , and protons. In addition, 'neutral beams' have been suggested (e.g. neutrons, Atoyan & Dermer 2004). The latter hypothesis requires that the direction into which the jet is launched changes with time to account for large scale bending and discrete deflections such as those in 3C 120 and 3C 390.3. Real jets may be made of several components, or may involve the transition of a jet dominated by one component into a jet dominated by another; e.g. a class of models postulates that an initially electromagnetic jet transforms into a particle dominated jet further downstream.

## 1.2 Jet formation, structure and propagation

**JET FORMATION** Jets are believed to be launched from accreting supermassive black holes and powered by either the gravitational energy of accreting matter that moves toward the black hole or, in the Blandford-Znajek process (Blandford & Znajek 1977), by the rotational energy of a rotating black hole. In the first case, jets may either be launched purely electromagnetically Blandford (1976), Lovelace (1976), or as the result of magnetohydrodynamic processes at the inner regions of the accretion disk (Begelman, Blandford & Rees 1984; Blandford & Payne 1982; Koide, Shibata & Kudoh 1999). In the Blandford-Znajek process, the black hole rotating in the magnetic field supported by the accretion disk gives rise to a Poynting flux. Most models of jet formation face the  $\sigma$ -problem ( $\sigma$  is the ratio of electromagnetic energy density to particle energy density), namely that they predict a Poynting flux dominated energy transport by a strongly magnetized or high- $\sigma$  plasma, while pc scale observations indicate that the jets consist of particle dominated, low- $\sigma$  plasma (Celotti & Fabian 1993; Kino, Takahara & Kusunose 2002; Krawczynski, Coppi & Aharonian 2002). Understanding the launching of jets may thus require the solution of two problems: the launching of a magnetically dominated outflow, and the conversion of such an outflow into a particle dominated jet. The latter transition is poorly understood, and requires more theoretical work.

The process of jet formation will have an impact on the steadiness of the jet-flow, and will affect the amplitudes and time scales of jet luminosity variations. Modulations of the power output are believed to cause the large amplitude brightness variations of the (unresolved) X-ray and  $\gamma$ -ray emission from blazars (Spada et al. 2001, Tanihata et al. 2003). Large amplitude variations on time scales of thousands of years may be responsible for the radio, optical and X-ray knots observed in many kpc-scale jets (Stawarz 2004, Stawarz et al. 2004), and the bright X-ray flare of the M87 jet (Harris et al. 2006). Several recent studies have shown that the flaring activity of AGN can be described in the language of noise processes (Uttley, McHardy & Vaughan 2005); i.e. the study of power spectra.

Blazar flares show that the noise process that drives flares has a rising amplitude of the power spectrum on the relatively long time scales of a few years. If jet knots reflect nuclear variability, it would require substantial power at much longer time scales (red noise) which of course are not available for direct observation.

**TRANSVERSE JET STRUCTURE** In addition to the obvious uncertainties as to the identity of the jet medium and its bulk velocity, several jet models involve jet structure perpendicular to the jet axis. Radio observations of transversely resolved jets (e.g. Laing & Bridle 2004; Lara et al. 2004; Pushkarev et al. 2005; Swain, Bridle & Baum 1998) and theoretical models of the core emission of blazars (Chiaberge et al. 2000) indicate a velocity gradient across the jet. Simple models use a two-zone structure, a fast moving spine that carries most of the jet energy, surrounded by a slower sheath, each with a characteristic value of  $\Gamma$  (Chiaberge et al. 2000). Laing & Bridle (2004) assume a gradual decline of  $\Gamma$  from the jet center to the outer parts of the jet: i.e. many layers with different velocities. If the velocity difference between layers is large, the particles in some layers see the relativistically boosted photons from other layers, resulting in an increase of the IC emission (Ghisellini, Tavecchio & Chiaberge 2005). A wealth of different jet structures has been proposed and studied in the framework of explaining the prompt and afterglow emission from Gamma-Ray Bursts (e.g. Graziani, Lamb & Donaghy 2006) and some of these may be relevant to kpc scale jets.

The fact that jets may have a complex structure is important for interpreting the observational data. For example, the dominance of the bright jet over the dim counter-jet in a number of sources was previously thought to constrain the bulk Lorentz factor of the jets (e.g. Wardle & Aaron 1997). However, the observations may merely show that most of the radio emission comes from a slow moving plasma, and thus may not constrain the bulk Lorentz factor of the jet component that carries most of the jet energy and momentum. The boundaries between jet layers of different velocity may accelerate particles (Stawarz & Ostrowski 2002) and are of special interest for jet stability considerations.

**JET PROPAGATION AND THE OCCURRENCE OF KNOTS** The origin of jet knots (localized brightness enhancements) and the mechanism that controls the location, strength, and longevity of the shocks thought to be responsible for the existence of knots, have not yet been identified unambiguously. It is important to remember however, that there is probably more than one type of knot and that there are several suggested methods of producing brightness enhancements in addition to the conventional explanation of particle acceleration at shocks. In the case of the M87 jet (fig. 3), the inner knots, D, E, and F appear quasi regular in size and spacing suggesting a possible origin associated with standing waves similar to those described by Beresnyak, Istomin & Pariev (2003), or by the elliptical mode Kelvin-Helmholtz instability (Lobanov, Hardee & Eilek 2003). Quite different are the knots A and C for which steep, quasi-planar gradients in radio brightness suggest reverse and forward shocks (see comment on shocks in the sidebar). Note however that Bicknell & Begelman (1996) have devised a detailed model of the M87 jet. They argue that all the knots can be explained by oblique shocks, with the apparent differences being ascribed to relativistic effects. Their model requires the angle between the jet axis and the line of sight to be  $30^\circ$  to  $35^\circ$ , a value substantially larger than the  $10^\circ$  to  $20^\circ$  required by the observation of fast moving blobs downstream from the leading edge of the knot HST-1 (see sec. 3.1.1).

---

### Forward &

### Reverse Shocks:

One sort of shock can arise from the interaction of a fast medium overtaking a slower medium. In the frame of the contact discontinuity separating the two media, a forward shock propagates downstream into the slower moving medium and a reverse shock propagates upstream into the faster moving medium. Particle acceleration can be associated with both. The structure of knot C in the M87 jet (with a large gradient in brightness, falling rapidly moving downstream) serves as an example of a forward shock, and the expected behavior of a reverse shock is exemplified by knot A (fig. 3).

---



\*

Figure 1: An HST image of the jet in 3C273.

One of the alternative explanation of knots is that knots in relativistic jets could be manifestations of a change in the beaming factor. The relativistic beaming factor,  $\delta$  depends both on  $\Gamma$  and on the viewing angle,  $\theta$  (the angle between the jet axis and the line of sight in the observer's frame):

$$\delta^{-1} = \Gamma(1 - \beta \cos \theta). \quad (1)$$

If the jet medium moves in a straight line so that  $\theta$  is fixed, an increase in  $\delta$  requires a significant increase in  $\Gamma$ . While we can imagine plausible ways to lower  $\Gamma$ , the critical question is, are there ways to increase  $\Gamma$  far from the central engine? This would entail a supply of energy such that the total power flow could decrease yet  $\Gamma$  could increase (e.g. by converting some power from the flow as in magnetic reconnection). Sikora et al. (2005) discuss this scenario, but deal only with the situation close to the black hole. While there is circumstantial evidence for acceleration of jet features on pc-scales (e.g. Hardee, Walker & Gómez 2005) and it is generally accepted that both FRI (Laing & Bridle 2002a) and quasar (Wardle & Aaron 1997) jets decelerate on pc to kpc scales there is no indication that significant jet acceleration occurs on kpc scales which may be required for some IC models of X-ray emission.

If the jet medium is allowed to significantly change its direction, modest changes in  $\theta$  can produce large changes in  $\delta$ . On VLBI scales, there has been a long standing debate on ballistic vs. curved trajectories. On the kpc scale the question arises: does the medium move in a straight or gently curved path, or might it follow a helical pattern controlled by a field structure of the same topology? If the latter case holds, the changes in brightness along the jet could be explained by beaming effects and some of the problems for high  $\Gamma$  jet models, such as excessive jet length, would be mitigated. Bahcall et al. (1995) remark on the apparent helical morphology of the HST image of 3C 273 (fig. 1) and Nakamura, Uchida & Hirose (2001) argue for a 'torsional Alfvén wave train' moving out to large distances from the central engine as a method of controlling the large scale structure. There are of course numerous examples of large scale bending (e.g. 3C 120: Walker, Benson & Unwin 1987) and discrete deflections (e.g. 3C 390.3 Harris et al. 1999); but in these cases we would anticipate deceleration only.

**TERMINAL HOTSPOTS** Terminal hotspots, like knots, are thought to be localized volumes of high emissivity which are produced by strong shocks or a system of shocks. The somewhat hazy distinction between hotspots and knots is that downstream from a knot, the jet usually propagates much as before, whereas at the terminal hotspot, the jet itself terminates and the remaining flow is thought to create the radio lobes or tails. Thus the underlying jet medium must suffer severe deceleration and the outward flow from the hotspot is non-relativistic and is not confined to a small angle. This is patently not true for the so called 'primary' hotspots in double or multiple systems. Instead of a terminal shock, primaries (and also aberrations such as hotspot B in 3C 390.3 North) may have oblique reflectors in essence, although the actual mechanism for bending might be more akin to refraction. For an extensive discussion of the differences between knots and hotspots, see Bridle et al. (1994).

---

**Fanaroff-Riley**

**class:** FRI radio galaxies are of lower radio luminosity than FR II's and quasars, and the brighter radio structures are close to the nucleus.

---



---

**VLBI:** Very Long Baseline

Interferometry: The technique of aperture synthesis in which the component radio telescopes are not physically connected, thereby permitting the use of inter-continental baselines resulting in synthesized beam sizes of milli arcsecs.

---

Knots are a common property of FRI jets and generally do not lead to a total disruption of the jet which maintains its identity downstream, be it relativistic or not. What we call knots in quasar jets, may have little in common with FRI knots given their relative physical sizes (fig. 6).

Insofar as the X-ray emission mechanism is concerned, the initial X-ray detection of the Cygnus A hotspots (Harris, Carilli & Perley 1994) was accompanied with a demonstration that synchrotron self Compton (SSC) emission provided a consistent explanation if the average magnetic field strength was close to the equipartition value under the assumption that the relativistic particle energy density was dominated by electrons, not protons. Essentially all the emission models for jet knots, on the other hand, have shown that SSC emission is completely inadequate to explain X-ray emission unless the magnetic field is orders of magnitude less than the equipartition value.

As the number of hotspot detections increased from CXO observations, many were found to be consistent with SSC predictions but a significant number appeared to have a larger X-ray intensity than predicted. This excess could be attributed to a field strength well below equipartition, IC emission from the decelerating jet 'seeing' Doppler boosted hotspot emission (Georganopoulos & Kazanas 2003), or an additional synchrotron component (Hardcastle et al. 2004a). The last named authors show that the strength of the excess correlates with hotspot luminosity in the sense that the strongest hotspots are consistent with SSC emission whereas the weaker radio hotspots required the extra synchrotron component.

For many distant and/or faint jets, it is often difficult to be certain that a feature is a knot, a hotspot, or even a lobe. In some extreme cases, the true nature of even bright hotspots is ambiguous. An example is the double hotspot system in 3C351 shown in fig. 2. Displaced from the north radio lobe is a double hotspot to the NE of the core. These are bright at radio and X-ray bands. The southern radio lobe has only a weak hotspot with at most 4% of the radio intensity of the NE hotspots at 1.4 GHz. Thus the double hotspot has the hallmarks of relativistic beaming in spite of the commonly held view that hotspot radiation is not beamed (see however Dennett-Thorpe et al. 1997, for a discussion of beamed emission from hotspots). Given the fact that these bright features are not located at the outer edge of the lobe, perhaps they are knots in a jet very close to our line of sight.

### 1.3 Entrainment and Collimation

Long-standing problems for low-loss jets include the suppression of mixing with ambient material and the collimation and stability of jets (Hughes 1991). The process of entrainment of ambient material is closely related to the process of jet deceleration. Both processes have been studied observationally (e.g. Laing, Canvin & Bridle 2003) and numerically (e.g. Rossi et al. 2004). Possible mechanisms causing entrainment include velocity shear and Kelvin-Helmholtz instabilities (Bodo et al. 2003). Laing, Canvin & Bridle (2003) have studied FRI radio galaxies assuming that the two sides of the jets are intrinsically identical and that the observed differences in radio brightness and polarization are caused by the viewing angle and relativistic beaming effects. They find the velocity of the jet plasma decreases moving away from the jet axis and that this velocity shear decelerates the jet substantially. These arguments purport to demonstrate that there is a clear distinction between FRI and FR II radio galaxies insofar as their

---

### Two-Zone Models

In many areas of jet modeling, it is often the case that a simple, single power law or a simply defined emitting region is inadequate to provide all the observed emissions. Thus we are tempted to invoke another (spatial) region or a second spectral component. In almost all cases, this is done with the tacit assumption that the second component is (or can be) detected in only one channel: i.e. either synchrotron or IC. We need to realize that when we introduce a two zone model, it precludes further analyses unless there is some hope of observing each zone in both channels. Some examples of current two zone models are the spine/sheath jet model (e.g. Celotti, Ghisellini & Chiaberge 2001); the idea that jets contain regions of high and low magnetic field strengths, with relativistic electrons moving between these regions; and the introduction of a second spectral component to explain hard X-ray (Harris et al. 1999) or optical (Jester et al. 2005) spectra.

---

jet properties are concerned. Since the powerful jets of FRII radio galaxies and quasars are able to escape the high ambient density of their host galaxies and maintain their collimation out to the prominent hotspots, it is inferred that they suffer less entrainment and deceleration than FRI jets (Bicknell 1995).

Collimation of jets has to be addressed both on sub-parsec scale during the process of launching the jet and on kpc-scales to explain the remarkable stability of jets. Tsinganos & Bogovalov (2002) for example consider the former problem and demonstrate collimation for a relativistic component by a second, non-relativistic less-collimated outflow (wind). Other collimation mechanisms include confinement by magnetic fields (Sauty, Tsinganos & Trussoni 2002), ram pressure of the ambient medium (Komissarov 1994), and by radiation (Fukue, Tojyo & Hirai 2001).

#### 1.4 Particle Acceleration and Emission Mechanisms

The Chandra X-ray observatory increased the number of jets with X-ray emission from a handful to  $\approx 50$  sources. Of these, 60% are classified as high-luminosity sources (quasars and FRII radio galaxies) and the remaining are low-luminosity sources (a mix of FRI's, BL Lac's and a Seyfert galaxy). The observations indicate that the radio to X-ray emission from low-luminosity FRI sources can be explained by synchrotron models, while that from the high-luminosity FRII sources requires multi-zone synchrotron models, synchrotron and IC models, or more exotic variants.

**SYNCHROTRON MODELS FOR FRI GALAXIES** For low-luminosity (FRI) radio sources, there is strong support for the synchrotron process as the dominant emission mechanism for the X-rays, optical, and of course radio emissions. Among the arguments supporting this view are the intensity variability found for knots in the M87 jet (Harris et al. 2006); the fact that in most cases the X-ray spectral index,  $\alpha_x$  is  $> 1$  and significantly larger than the radio index,  $\alpha_r$ ; and the relative morphologies in radio, optical, and X-rays. For the sorts of magnetic field strengths generally ascribed to jet knots (10 to 1000  $\mu\text{G}$ ), synchrotron X-ray emission requires the presence of electrons of energies in the range  $10^7 < \gamma < 10^8$ . As the highest energy electrons cool in equipartition magnetic fields on time scales of years, the observations of single power-law spectral energy distributions extending all the way from the radio to the X-ray regime pose the problem of why there is no sign of radiative cooling. A possible solution may be that electrons escape the high-magnetic field emission region before they cool.

The radio to X-ray observations require the presence of one or more populations of high energy electrons (or protons if proton synchrotron emission is viable, (Aharonian 2002)). A common assumption is that the particles are accelerated at strong magnetohydrodynamic (MHD) shocks by the Fermi I mechanism (Bell 1978, Blandford & Ostriker 1978)(see also the review by Kirk & Duffy 1999). However, there are several uncertainties. First we cannot be sure that the Fermi process is relevant since if the jet is strongly magnetized with a tangled field geometry, shock acceleration is not as effective as for strong shocks which can exist when the field does not dominate. Next, the uncertainty of the bulk Lorentz factor of the jet medium means that we can't be sure that  $\Gamma$  is large enough to allow the possibility of relativistic shocks. Finally, even if the bulk velocity of the jet is relativistic, it is still possible to have non-relativistic shocks in the jet frame. For mildly relativistic shocks, Fermi I shock acceleration is more complicated than

---

#### Energy Losses & Halflives

Relativistic electrons loose energy via several processes. For both synchrotron and inverse Compton radiation, the rate of energy loss is  $\propto E^2$  ( $E$  is the electron's energy). For these loss channels, the time it takes to loose half the energy ('half-life') is  $\propto E^{-1}$ .

---



is the case for the non-relativistic regime, and it is not yet well understood (Kirk & Duffy 1999)).

**Distributed Acceleration** For FRI jets such as that in M87 (fig. 3), X-ray emitting electrons with  $\gamma \approx 10^7$  will cool on time scales of a few years, and optical and UV emitting electrons will cool on time scales of a few decades. Thus, interpreting the X-ray and optical emission from these sources as synchrotron emission implies that the emitting regions cannot be much larger than the electron acceleration regions. For bright knots which have traditionally been associated with strong shocks in the jet flow, these “life-time constraints” can easily be accommodated. However, Chandra detected several jets with quasi-continuous emission along the jet (e.g. Cen A, Kataoka et al. 2006) suggesting that electron acceleration may be spatially distributed rather than being restricted to a few bright knots. Wang (2002) finds that plasma turbulent waves can be a mechanism for efficient particle acceleration, producing high energy electrons in the context of blazar jets. Nishikawa et al. (2005), Stawarz & Ostrowski (2002) propose turbulent acceleration in a jet’s ‘boundary’ or ‘shear’ layer surrounding the jet spine. Stawarz & Ostrowski (2002) also argue that the resulting electron energy distribution should show an excess near the high energy cutoff, thereby producing a harder X-ray spectrum than would be expected based on the extrapolation of the radio and optical data.

Other explanations for the quasi-continuous emission include low-level IC/CMB emission of low-energy electrons (see the discussion in the next paragraph) and synchrotron emission from electrons accelerated by magnetic reconnection. However, if the knot emission is produced by synchrotron emission from shock-accelerated electrons and the continuous emission has another origin, one might expect that the two jet regions would show markedly different spectral energy distributions. Measurement of X-ray spectral indices of the continuous emission is usually difficult, because of the fewer photons available for analysis. In the case of M87, Perlman et al. (2003) find no change of  $\alpha_x$  between the knots and the quasi-continuous emission within a statistical accuracy of  $\pm 0.15$  in the X-ray spectral index.

**Departures from power law spectra** One of the primary reasons that IC/CMB models are preferred over synchrotron models for most FR II radio galaxies and quasars is the so-called ‘bow-tie problem’. Conventional synchrotron spectral energy distributions call for a concave downward spectral shape, allowing for spectral breaks to steeper spectra at higher frequencies and eventual high frequency cutoffs. Thus we expect  $\alpha_x \geq \alpha_{ox}$  ( $\alpha_{ox}$  is the spectral index between optical/UV and X-ray). When this is not the case, the ‘bow-tie’ showing the X-ray flux density and allowed range of  $\alpha_x$  does not permit a smooth fit of a concave downward curve and instead requires a flattening of the X-ray spectrum. Examples are provided in fig. 4 which shows the SED’s for 3 knots in the 3C273 jet. The bow-tie problem is more common for FR II radio galaxies and quasars but is also found for some of the FRI radio galaxies.

In addition to the hypothesis of a second spectral component, there have been two suggestions for accommodating this behavior with synchrotron emission. The first is that mentioned above: boundary layer acceleration (Stawarz & Ostrowski 2002) producing a flatter spectrum for the high energy part of the electron spec-

---

**SED:** Spectral Energy Distribution: To describe the continuum spectrum of a feature,  $\log(\nu \times \text{flux density})$  is plotted against  $\log \nu$ . We use the term also for  $\log(\text{flux density})$  vs.  $\log \nu$ .

---

trum. The other suggestion is restricted to the case where IC dominates the  $E^2$  losses. Dermer & Atoyan (2002) argue that for the highest energy electrons, IC losses are reduced by the lower Klein-Nishina cross section so that the top end of the electron distribution experiences a reduced loss rate and thus an excess above the expected distribution builds up at high energies producing a hard synchrotron spectrum at X-ray frequencies. Although this is a clever method of solving the bow-tie problem, in order to work, the photon energy density in the jet frame,  $u'(\nu)$  must be larger than the magnetic field energy density,  $u(B)$ . To realize this, a  $\Gamma^2$  boosting of the CMB is required, and the practical result is that by invoking the necessary  $\Gamma$ , you will already produce the observed X-ray emission by the IC/CMB process.

**EMISSION MODELS FOR FRII GALAXIES AND QUASARS** The most pressing problem for X-ray emission from relativistic jets is the emission mechanism for the powerful jets from FRII radio galaxies and quasars. As mentioned above, the radio to X-ray spectral energy distributions of most of these sources cannot be described by a one-component synchrotron model. Such models predict a spectral energy distribution which softens at high energies. In terms of spectral indices, we expect  $\alpha_x \geq \alpha_{ox}$ , whereas the Chandra observations showed that  $\alpha_x < \alpha_{ox}$  for many quasar jets. The most popular explanation is the IC model put forth by Celotti, Ghisellini & Chiaberge (2001) and Tavecchio et al. (2000). The observed large ratios of X-ray to radio luminosities are explained by postulating very fast jets with high bulk Lorentz factors  $\Gamma$ . Relativistic boosting increases the energy density of the CMB in the jet frame:

$$u'(\text{CMB}) = 4 \times 10^{-13} (1+z)^4 \Gamma^2 \text{ erg cm}^{-3}. \quad (2)$$

In this way, a single population of electrons is able to produce the radio and optical synchrotron emission in a magnetic field close to equipartition ( $B_{eq}$  generally less than  $100 \mu\text{G}$ ), and the IC X-ray emission by scattering off the relativistically boosted CMB.

While we evaluate the various difficulties confronting the IC/CMB model in the final section of this review (4.2), we would like to emphasize here that the IC/CMB model requires two key-ingredients for which there is at present no independent observational verification: enough low-energy electrons and highly relativistic plasma motion on kpc-scales. Analysis of the spectral energy distributions of several FRII sources shows that electrons with Lorentz factors  $\gamma' \approx 100$  produce the observed X-rays: (e.g. Harris & Krawczynski 2002, eq. B4):

$$\gamma' = \sqrt{\frac{6.25 \times 10^{-12} \nu_{ic}(obs)}{(1 + \mu'_j)\delta\Gamma}}. \quad (3)$$

where the prime is used to denote quantities in the jet-frame,  $\mu'_j$  equals  $\cos(\theta')$  and  $\theta'$  is the angle between the jet direction and the line of sight. The uncertainties of extrapolating the electron spectrum to low energies is illustrated in fig. 5 which shows the spectrum of the knot in the jet of PKS0637-752. The low-energy electrons responsible for the X-ray emission produce synchrotron emission in the 1-30 MHz range, well below frequencies available from the Earth with reasonable angular resolutions. For this example we have used  $\Gamma=10$ , which is the value required for the IC/CMB model (Celotti, Ghisellini & Chiaberge 2001; Tavecchio et al. 2000). The actual electron spectrum could flatten significantly for  $\gamma \leq 3000$  or even suffer a low energy cutoff. In that case there would be fewer electrons than

calculated, and the required value of  $\Gamma$  would have to be increased to compensate. It is even conceivable that the electron spectrum could steepen at low energies and the required  $\Gamma$  would be much smaller than estimated. Our ignorance of the low end of the electron spectrum is very general; only in sources with very high values of magnetic field strength do ground based radio data begin to give us the required information.

On the positive side, the IC/CMB model avoids the 'far-from-equipartition' requirement of models which explain the high X-ray fluxes as synchrotron self-Compton emission from electrons up-scattering long-wavelength synchrotron photons into the X-ray band (e.g. Schwartz et al. 2000). Furthermore, it does not require the ad-hoc introduction of additional particle components, required by multi-zone synchrotron models (e.g. Harris et al. 1999).

## 2 Physical Comparisons of Resolved X-ray Jets

We are used to looking at images of jets that fit nicely on the page, be they Galactic micro quasars, jets from relatively local FRI radio galaxies, or jets from quasars with substantial redshifts. We are struck by a number of similarities and are tempted to consider them all to share fundamental properties. In an effort to sharpen our perspective, we have devoted this part of the review to presenting the observed and deduced parameters for the X-ray jets known to us. Most of these data exist in the literature, but we have adjusted published values, where necessary, to conform to the currently standard cosmology:  $H_0=71 \text{ km s}^{-1}$ ;  $\Omega_m=0.3$ ; and  $\Omega_\Lambda=0.7$ . Gathering these data will allow us to compare physical sizes and apparent luminosities.

In fig. 6 we show the relative sizes of 3 jets: M87, 3C273, and PKS1127-145. Although the indicated sizes (1.6, 56, and 238 kpc, respectively) are projected sizes, it can be seen that the entire jet of M87 would easily fit within a single knot of the 3C273 jet. Note also that a single  $0.049''$  pixel in the top panel corresponds to a few pc, the scale of VLBI jets and also comparable to the total size of jets from microquasars in our galaxy. Given the vast range of scales, can we really expect similar physical processes to operate all the way from pc to Mpc scales?

### 2.1 Gross jet properties

In Table 1 we list parameters for X-ray jets of low radio power sources from the XJET website<sup>3</sup> (2005.6), and Table 2 contains the data for the more powerful sources classified as quasars or FRII radio galaxies. We have not included sources if only the terminal hotspots and/or lobes have been detected in X-rays. In almost all cases, the division between the two tables corresponds to how the original investigators interpret the X-ray emission process. All the entries in Table 1 are ascribed to synchrotron emission except for Cen B, and similarly the jets of Table 2 are described on the basis of the IC/CMB model except for PKS2152-69 for which Ly, De Young & Bechtold (2005) suggested thermal emission; Pictor A, PKS 1136-135 and 3C 273 for which both synchrotron and IC/CMB have been suggested; and 1928+738 and 3C403 which have been ascribed to synchrotron emission.

The projected jet length, both in arcsec and kpc should be accurate to about

---

<sup>3</sup><http://hea-www.harvard.edu/XJET/>

10%; it is meant to describe the length of the X-ray jet as detected by the CXO and not the total length of the radio jet. The apparent X-ray luminosity is derived from the observed flux or flux density, assuming  $\alpha_x=1$ . As pointed out by Lister (2003), such luminosities are not directly useful for correlations since we are dealing with relativistic beaming which alters the jet frame luminosity, depending on  $\Gamma$  and  $\theta$ . The value of  $\alpha_x$  given is a published value, either for the whole jet, or from a brighter knot. If a reasonable estimate of the angle of the jet to the line of sight is given in the literature, it is quoted here. For a number of the quasars,  $\theta$  is estimated from the IC/CMB calculation, and is thus model dependent; for others, it is estimated from VLBI studies. The resulting deprojected length suffers from similar uncertainties.

## 2.2 Evaluation

In fig. 7 we show a plot of the observed parameters, jet length (projected) and observed (i.e. assuming isotropic emission) X-ray luminosity,  $L_x$ . This plot conforms to the common perception that quasars have powerful jets and are generally longer than those of FRI galaxies. Perhaps the only surprise is the gap with no jets lying between  $10^{42}$  and  $10^{43}$  ergs  $s^{-1}$ . The lower right is sparsely populated partly because in a large fraction of FRI jets, only the inner segment is detected in X-rays. The upper left is empty because short jets at typical quasar redshifts will be difficult to resolve from the nuclear emission with arcsec resolutions. A separation of  $\approx 2''$  is required to detect a jet close to a bright quasar, and at a typical redshift of 0.5, this already corresponds to 10kpc.

The FR II radio galaxies have projected sizes comparable to those of the quasars, but are of lower apparent luminosity. The weakest jet (lower left corner) is M84 for which X-ray emission has been detected in the very inner part of the radio jet. 3C129 is quite similar, and joins Cen A, both points lying to the lower left of the main clump of FRI's.

This sort of plot is useful for comparative purposes, but not for interpretation because  $L_x$  is only an apparent luminosity and not the true luminosity in the jet frame and also because the length is a lower limit because of projection.

For a subset of the sources plotted in fig. 7, some reasonable estimate for the angle between the line of sight and the jet has been published. Since most of these jets are sensibly straight on kpc scales (3C120 being a notable exception), we can obtain a deprojected length. For most of these, an estimate of the beaming factor is also available. For the majority of the quasars, the value of  $\delta$  given in Table 2 is model dependent since it is the beaming factor required for the IC/CMB model. For the FRI and FR II radio galaxies, the  $\delta$  values are derived from various lines of arguments based on geometry of the lobes, VLBI superluminal motions, and other more or less reliable methods. Assumed  $\delta$ 's for the FRI jets are: 1.3, 3C31 and M84; 3.5, M87 and 3C371; 4, Cen A; and 3, 3C346. However, all beaming factors are suspect and the corresponding uncertainty will most likely introduce scatter in plots such as fig. 8 which plots  $L'_x=L_x(obs)/\delta^4$  against  $length(obs)/\sin\theta$ .

The main purpose of fig. 8 is to demonstrate that with the 'current community interpretation' (i.e. FRI jets come from synchrotron emission whereas quasar jets are dominated by IC/CMB emission), FRI jets and quasar jets are more clearly separated on the basis of size rather than luminosity. Parameters for the smallest quasar jets (the group of 5 around  $\log L'_x=42$ ,  $length=70kpc$ ) are less secure since the jet emission is only of order one resolution element from the quasar core

emission for these sources.

$L'_x$  values are compromised by model dependency. If quasar jets were to come from synchrotron emission instead of IC/CMB emission, the appropriate  $\delta$  could well be of order 3 or 4 (similar to that for FRI's, and adequate to explain the jet one-sidedness) instead of typical values like 10. Thus the luminosity correction when moving to the jet frame would be closer to a factor of 100 than 10,000 and the plot would be closer to a scaled version of fig. 7.

For both of these figures we need to remember that 'low-power' and 'high-power' sources are so divided according to their total radio luminosity. When we plot the jet luminosity we are dealing with a parameter that quantifies the jet loss, not the jet power. Since FRI jets are commonly thought of as being 'lossy', the underlying assumption is that a larger fraction of the FRI jet power is radiated than is the case for FR II jets. Thus both the characteristic power and the fractional energy lost to radiation for both classes of sources are 'free' parameters and the resulting luminosities (luminosity = total jet power  $\times$  fractional loss to radiation) would not necessarily be expected to be similar as in fig. 8.

### 3 Observations of Resolved Jets

#### 3.1 Relevant Radio and Optical Considerations

In addition to the critical role of radio and optical flux densities, which complement the X-ray intensities in defining the SED's of jet knots, these longer wavelengths provide 2 critical capabilities for jet observations: higher angular resolution than that of the CXO, and polarization. Moreover, in most cases, we are confident that we can interpret the data on the basis of synchrotron emission rather than being faced with the uncertainty of IC vs. synchrotron emission, as is the case for the X-rays.

For the SED's, the IR-optical-UV data are usually those which determine if a synchrotron spectrum (broken power law with high energy cutoff) can be used to describe the radio to X-ray data. For example, Jester et al. (2005) find a spectral flattening from HST data in the 3C273 jet which is the basis for the claim that a simple synchrotron spectrum cannot fit all the data. Often the optical upper limit for a non detection is used to preclude a single synchrotron component whereas if no optical data were available, the radio and X-ray data could have been interpreted as a single (broken) power law.

There are at least two observational problems affecting the construction of SED's. The first is the uncertainty that our photometry is measuring the same entity in all bands. The CXO resolution is significantly worse than that of the HST so to gather the counts for photometry, one needs at least a circle with radius of  $0.5''$ . Thus when measuring the SED of the knots in e.g. 3C273 (fig. 1), we implicitly assume that the X-rays are coming from the same emitting volume as the optical/radio, and not from some additional volume such as a sheath around knots.

The second uncertainty is the absorption correction which mainly affects the UV and soft X-ray data, and depends not only on the column density to the source, but also on the gas to dust ratio.

**3.1.1 MORPHOLOGY AND POLARIZATION AT KPC SCALES** One of the more significant advances in understanding radio jets has been achieved by Laing & Bridle (2002a,b). For the case of FRI jets for which both sides are visible and



well resolved, they have been able to use the laws of energy and momentum conservation to solve for all the physical jet parameters assuming that the observed differences in brightness and polarization between the two sides are caused by relativistic effects only (see Königl 1980, for a general discussion of relativistic effects). For 3C31 they find  $\beta=0.8$  to  $0.85$  initially, then decelerating to  $\beta=0.2$  at a few kpc's, with loading by entrainment being the cause of the deceleration. The solution requires cross jet velocity structure: the outside has to be going slower than the center. This is consistent with, but does not require, a simple 'spine/sheath' structure.

Optical and radio polarization have also been used to study the field configuration in relation to the properties of internal shocks in jets. For example, Perlman & Wilson (2005) find that the peaks in X-ray brightness in the M87 jet coincide with minima of the optical polarization. They conclude that this is consistent with the location of internal shocks which both produce the X-ray emission via particle acceleration and change the magnetic field direction. The observed reduction in polarized signal would then be a result of beam smearing over a region of swiftly changing field direction.

Other notable progress coming from optical data includes Biretta, Sparks & Macchetto (1999) who found features moving at  $\approx 6c$  downstream from M87/HST-1 (the same knot which later flared by a factor of 50 across the spectrum). This demonstrates that at least mildly relativistic velocities persist to kpc scales. Several investigators (see for example Macchetto 1996) have also noted that optical emission away from bright knots requires continuous acceleration processes since the  $E^2$  loss times are so short that the electrons responsible for the observed emission cannot travel from the shock locations; the same sort of argument was later deduced from similar morphologies observed at X-ray frequencies.

**3.1.2 PARSEC SCALE STRUCTURES** The most relevant aspect of VLBI work for X-ray jet physics is the accumulating database containing monitoring of a reasonably large sample of quasar, blazar, and BL Lac jets. The original work was the "2 cm survey" which has now become institutionalized on the web as MOJAVE<sup>4</sup>. These data provide a wealth of information such as the distribution of beaming factors and jet velocities (if one accepts the notion that observed proper motions of jet features reflect the underlying jet velocity and that the sources are at distances indicated by their redshifts). Kellermann et al. (2004) find apparent velocities  $\beta$  ranging from zero to 15, with a tail extending up to 30 for individual features. With assumptions about brightness temperatures, this can be translated to  $\Gamma$  values covering a similar range. If bulk velocities of this magnitude persist to kpc scales, one of the prerequisites of the IC/CMB model for X-ray jet emission will be satisfied.

Another VLBA monitoring project is described in Jorstad et al. (2005). They find a similar range for  $\Gamma$  using intensity variability timescales to estimate  $\delta$ , with most quasar components having  $\Gamma$  of order 16 to 18. In both of these works, there is ample evidence of non-ballistic motion: velocity vectors of components mis-aligned with the jet vector.

Gabuzda, Murray & Cronin (2004) have used the transverse polarization structure of jets resolved with VLBI to argue for a helical structure for the magnetic field governing the emitting region; circumstantial evidence for non-ballistic motions.

---

<sup>4</sup><http://www.physics.purdue.edu/astro/MOJAVE/>

Wardle et al. (1998) argued for jet composition being a pair plasma based on circular polarization inferences and Hirotani et al. (1999) suggested that two components in the jet of 3C279 were dominated by pair plasma on the basis of electron density arguments.

### 3.2 The X-ray Data

We will not cover inferences from unresolved X-ray behavior of cores, but concentrate on jet features for which we have some confidence that the radio, optical, and X-ray emission comes from the same emitting volume. We make the usual assumptions that all relativistic plasmas will emit both synchrotron and IC radiation and since most/all X-ray jets are one sided, and these sides are the same as the those which have VLBI superluminal jets,  $\Gamma > 1$ , but not necessarily  $\geq 5$  (for kpc scales).

**3.2.1 JET STRUCTURE** So far, there is very little transverse structure available from X-ray data. A notable exception is knot 3C120/k25 (Harris, Mossman & Walker 2004) which is resolved into 3 components. The jet of Cen A is well resolved since it is the nearest jet source (Kraft et al. 2002). M87/knots A, B, and C are a bit larger than the point spread function (Perlman & Wilson 2005) and Marshall (private communication) reports that several features in the jet of 3C273 are also resolved by the CXO.

In general, there is good correspondence between jet knots mapped in the radio, optical, and X-ray bands. For both IC and synchrotron emission models, this is expected in first-order approximations if there is a single relativistic electron distribution responsible for all observed emissions. Relative intensities between bands can vary depending on the relative magnitudes of energy densities in the magnetic field and in the photons, as well as on the form of the electron distribution,  $N(E)$ , since different bands come from different segments of  $N(E)$ .

There are, however, a few cases of gross mis-alignment between an X-ray feature and emissions at lower frequencies. In the M87 jet, beyond knot C (upper right of fig. 3) the radio jet makes a sudden excursion to the north downstream from a sharp gradient in radio brightness (in the opposite sense to that of the leading edge of knot A). Although there is weak radio emission downstream of this radio edge, the X-ray brightens. One interpretation might be that the radio jet encounters an 'obstacle' causing an internal shock and a jet deflection. The X-ray emission would then come from the obstacle, and not properly be associated with the jet itself. A similar situation occurs just downstream of knot A in the jet of 3C273 where the radio jet deflects to the South before resuming its principal direction, whereas the X-ray, and in this case also the optical emission, continues further North along the main jet vector defined by knot A and the rest of the jet (fig. 9).

Another example of discrepant correspondence between radio and X-rays is Cen A (Hardcastle et al. 2003, 2004b, Kraft et al. 2002), shown in fig. 10. While many radio and X-ray features align well, albeit with quite different relative intensities, there are a few X-ray knots that have no obvious corresponding radio enhancements. For PKS1136-135 (Sambruna et al. 2004, 2002), the radio emission associated with the first bright X-ray knot ('A') is extremely weak; another example of the range of relative intensities between radio and X-ray emissions.

**Offsets** Another common, although not universal, effect is the offset between peak X-ray, optical, and radio brightness distributions when mapped with similar

angular resolutions. It is generally the case that when this occurs, the higher frequency brightness peaks at the upstream end of the knot, and the underlying cause seems to be a steepening of the spectra moving downstream (Hardcastle et al. 2003). A few examples are Cen A, fig. 10 for knot A2 at RA=13h 25m 29s; M87 knots D and F (fig. 3); and knot B in PKS1127-145 (fig. 11). For the nearby sources Cen A and M87, the magnitude of the projected offsets are of order tens of parsecs, whereas for PKS1127-145 at  $z=1.18$ , the observed offset is of order 10 kpc. Additional examples from the FRI category are listed in Bai & Lee (2003), a paper devoted to the offset effect.

For the simplest synchrotron scenario, if electrons were to be accelerated at a single location (i.e. a shock) and then be advected down the jet, all synchrotron bands should coincide insofar as peak brightness goes, even though downstream, we would expect to lose the highest energy electrons sooner than the lower energy electrons responsible for the radio emission. This statement assumes perfect angular resolution whereas normally, our beam sizes are not adequate to discern these structural differences. Thus even with the same angular resolution, the peak brightness of the X-ray emission, being centered on the shock, can occur upstream of the radio centroid which has been shifted downstream a bit since the downstream plasma will continue to produce radio emission (but not X-rays).

Another possibility to explain the observed offsets which is not fine-tuned to the beam size is an increasing magnetic field strength downstream from the shock, thereby enhancing the radio emissivity. While the physical scales for the nearby sources are reasonably consistent with these models (travel time matching  $E^2$  halflives), the 10kpc offset for PKS1127-145 (again assuming synchrotron emission) would most likely rely on the second explanation. It is also the case, as emphasized earlier, that whereas we expect the electrons responsible for the X-ray emission to travel no further than some tens of light years, there is emission between the bright knots in many jets, and this supports the presence of a distributed, quasi continuous acceleration mechanism (see sec. 1.4).

For the IC/CMB model, currently there is no reasonable explanation as to why the X-ray emission should drop off more rapidly than the radio/optical synchrotron emission since the X-ray producing electrons have  $\gamma \leq 200$ , and thus much longer halflives than the electrons responsible for the radio (and optical) emission. There are of course *ad hoc* possibilities such as a precursor shock system (or some other mechanism) which would accelerate copious numbers of electrons only up to some small value of  $\gamma$  like 1000.

**Progressions** Another effect which is closely associated with offsets is what we call “progressions”. This term is applied to those jets for which the X-ray intensity is highest at the upstream end, thereafter generally decreasing down the jet, whereas the radio intensity increases along the jet. Progressions are rather common; in Sambruna et al. (fig. 5 of 2004) this effect is shown for 7 quasars. The most striking example is 3C273 and profiles are shown in fig. 12. Note that the optical knots are of relatively constant brightness. If this jet were to be observed with a single resolution element, there would be a clear offset between peak brightnesses in the radio and X-ray which would most likely be comparable to the length of the bright part of the jet,  $\approx 6''$  (15 kpc). Referring to fig. 6, we see that the 3C273 jet is about the size of a single ‘knot’ in the PKS1127-145 jet. Thus we see that ‘progressions’ and ‘offsets’ can be considered to be two

manifestations of an underlying spectral behavior. Both offsets and progressions are observed in FRI and in quasar jets although the common explanations for the two classes differ. For synchrotron models an increasing magnetic field strength is posited, thereby increasing the synchrotron emissivity. For IC models, a gradual decrease in jet bulk velocity is assumed, leading to a diminishing  $u'(\nu)$  in the jet frame (Georganopoulos & Kazanas 2004).

**Emission between the knots** Although the conventional view of synchrotron jets is that electrons responsible for X-ray emission cannot propagate more than a few light years from their acceleration site, lower brightness emission is often detected between the brighter knots. In their survey of quasar jets, Sambruna et al. (2004, their sec. 4.3) remark on this attribute for PKS0605-085 and possibly also for 3C207 and PKS1136-135. Because of the lower brightness levels in both radio and X-ray bands, it has been difficult to obtain the data necessary to perform spectral tests for the emission mechanism. Quasi continuous jet emission is expected for the IC/CMB process whereas a synchrotron hypothesis would require continuous acceleration processes, as outlined in sec. 1.4.

**3.2.2 RELATIVE INTENSITIES AND SED'S** Combining radio, optical, and X-ray photometry to create a broad band spectrum is the standard method to discriminate between synchrotron and IC emission. Resting on the common assumptions of a power law distribution for the relativistic electrons and  $E^2$  losses affecting the highest energy electrons more severely than the lower energy electrons, the notion that a one zone synchrotron source must have a concave downward spectrum has been generally accepted. This approach can work even if only 3 flux densities are available (i.e. one radio, one optical, and the X-ray measurement), but can become stronger with more data, permitting estimates of the spectral index to be obtained within each band.

There are several variations of this test such as plotting  $\alpha_{ro}$  against  $\alpha_{ox}$  (e.g. Sambruna et al. 2004, fig. 4), or simply demonstrating that an optical upper limit lies below the line connecting the radio and X-ray data (e.g. Schwartz et al. 2006). Of the 34 quasars and FRII radio galaxies listed in Table 2, 9 have been shown by Sambruna et al. (2004) to have knots with  $\alpha_{ro} > \alpha_{ox}$  and another 8 have optical upper limits which preclude a simple synchrotron fit. Twelve of the sources do not yet have useful optical data available, and the remaining 5 consist of a few FRII radio galaxies and a couple of quasars for which some knots have spectra consistent with a synchrotron fit while others do not.

Although it is thus fairly simple to demonstrate that a simple (i.e. 'single zone') synchrotron spectrum fails to apply to most knots in quasar jets, once high quality data are available, serious problems arise also for the single zone IC/CMB models. Examples are spine-sheath models devised to benefit both from high and low  $\Gamma$  effects and 3C273 for which some knots seem to have  $\alpha_x > \alpha_r$ , contrary to the expectation that electron spectra will most likely flatten at low energies (Jester et al. 2006).

**3.2.3 VARIABILITY** Since the CXO has been providing X-ray photometry of jet components for only 6 years, to detect variability we require a small physical size abetted by a significant value of  $\delta$  to compress the elapsed time in our frame.

Thus, clear intensity variability has so far only been found in Cen A (Hardcastle et al. 2003) and M87 (Harris et al. 2006). This is not meant to preclude the possibility of detection of variability in larger structures which could well contain

small scale structure. If one were to ascribe the factor of 100 difference in apparent luminosities between 3C273 and M87 to a factor of 3 difference in  $\delta$ , then an event such as the flare in knot HST-1 of M87 (Harris et al. 2006) would be easily detected. The factor of 50 increase in the X-ray flux from HST-1 means that what was once an inconspicuous X-ray knot for a time outshone the remainder of the jet plus the unresolved core of M87.

Proper motion has been observed for radio features in Cen A (Hardcastle et al. 2003) and optical features moving at up to 6c downstream of HST-1 in M87 (Biretta, Sparks & Macchetto 1999). In both cases, the associated X-ray features align with stationary radio or optical components.

### 3.3 Jet Detection Statistics

In the standard picture of AGN unification (Urry & Padovani 1995), there are two main classes of AGN, low-power AGN (BL Lac objects and low-power radio galaxies) and high-power AGN (Quasars and high-power radio galaxies). The differences of AGN within each class are explained with a different degree of alignment between the line of sight and the symmetry axis of the AGN (assumed to be parallel with the AGN jets). BL Lac objects are interpreted to be the aligned versions of FRI radio galaxies, and steep spectrum radio quasars (SSRQ - sources with a radio spectral index  $\alpha_r, > 0.5$  at a few GHz) and flat spectrum radio quasars (FSRQ,  $\alpha_r, < 0.5$ ) are increasingly aligned versions of the FRII parent population. Urry & Padovani (1995) derive the luminosity functions of the beamed AGN from the luminosity function of the parent populations. For their specific source samples, their analysis indicates that FRII radio galaxies have jets with bulk Lorentz factors of between 5 and 40, and that SSRQs and FSRQs are FRIIs with jets aligned to within  $\sim 38^\circ$  and  $\sim 14^\circ$  to the line of sight, respectively. The bulk Lorentz factors of the FRI jets are less constrained but seem to be somewhat lower than those of the FRII jets, and the jets of their radio selected BL Lacs seem to be aligned to within  $12^\circ$  to the line of sight.

In this context, we now consider the sources with X-ray jets (see Tables 1 and 2). The low-power sources with X-ray jets are mostly FRI radio galaxies, except for 3C120, a Seyfert I galaxy and the two BL Lacs PKS0521-365 and 3C371. The high-power sources with X-ray jets are all classified as quasars except for the four FRII radio galaxies Pictor A, 3C219, 3C403 and PKS2152-69. Remarkably, almost all X-ray jets from the non-aligned FRI and FRII sources can be explained as synchrotron emission from mildly relativistic jets; Lorentz factors of a few are needed to explain the non-detection of counterjets. Most sources for which the simple synchrotron picture does not work are quasars. In this case, explaining the X-ray emission requires Lorentz factors on the order of 10 and viewing angles on the order of  $10^\circ$ . The IC/CMB interpretation of the X-ray emission thus indicates that the X-ray jets detected so far are similarly closely aligned to the line of sight as the average radio-selected FSRQs used in the FRII/quasar unification analysis described above.

Marshall et al. (2005), Sambruna et al. (2004) used the CXO to study the fraction of sources with X-ray jet emission for certain source samples. Sambruna et al. (2004) studied sources with bright 1.4 GHz radio emission and a radio knot detection more than  $3''$  away from the core. Out of a sample of 17 sources, X-ray jets were detected for 10 sources. Marshall et al. (2005) studied two samples of flat spectrum radio sources. One sample consisted of sources selected for their high



5 GHz flux density. The other sample consisted of sources with one-sided linear radio jet morphology. Out of 19 sources of the first sample, 16 were detected with short CXO observations. The detection probability in the second sample was lower, but this finding was not statistically significant.

The samples used in these "survey-type studies" were biased toward beamed sources. As the alignment of the sources is poorly constrained by the longer wavelength data, the high detection fraction with CXO cannot be used to argue for or against the IC/CMB model for those sources for which simple synchrotron models do not account for the X-ray emission.

As mentioned above, the radio spectral index can be used as an indicator of the jet orientation relative to the line of sight. A similar indicator is the lobe over core dominance at intermediate radio frequencies like 5 GHz. A test of the IC/CMB model is to check that the orientation parameters indicate an aligned jet for all quasars that exhibit the bow-tie problem. Indeed only for one source (PKS 1136-135) do we find at the same time  $\alpha_r \gg 0.5$ , lobe over core dominance and a SED which indicates a bow-tie problem. However, this source does not make a strong case against the IC/CMB model. Only knot B exhibits the bow-tie problem and close inspection of the radio-X-ray morphology shows that it may well be a hot-spot rather than a jet knot. We conclude that the IC/CMB scenario is not grossly inconsistent with other orientation indicators.

## 4 Discussion & Summary

### 4.1 Critique of the Synchrotron Emission Model

There seems to be little doubt that the X-ray emission from most or all jets of FRI sources is dominated by the synchrotron process. When SED's are available, they are consistent with concave downward fits. There are no problems with the synchrotron parameters such as magnetic field strength or energy requirements. Light curves for variable knots also support the synchrotron model even if the predictions for behavior at lower frequencies still need to be verified. The alternative of IC/CMB emission requires unreasonable beaming parameters such as angles to the line of sight which are too small compared to a host of other estimates.

Perhaps the most important implication to be deduced from FRI jets is the necessity for distributed emission rather than a finite number of shocks. While we don't doubt the evidence for strong, discrete shocks (e.g. a large gradient in radio brightness, often facing upstream), some additional process is required.

The most likely alternatives for the 'additional process' are the aforementioned 'distributed acceleration' and IC/CMB emission. As outlined in sec. 1.1, one of the candidates for the underlying jet 'medium' is electrons with  $\gamma <$  a few thousand. If that option were to be correct, then it could well be the case that even very modest values of  $\Gamma, \delta$ , and  $\theta$  would suffice for an IC/CMB model of inter-knot emission, and many of the problems of this process for knots would not be present. It is likely that sufficient data have now accumulated in the relevant archives that this test could be performed for a number of the brighter jets with well defined knots.

To explain jet segments devoid of detectable emission, this scenario would indicate that jets are inherently intermittent. Aside from testing this suggestion by careful photometry, spectral analysis, and calculation of beaming parameters,

it would be a somewhat unbelievable coincidence if the energy spectral index,  $p$ , [ $N(\gamma) \propto \gamma^{-p}$ ] were to be the same for the postulated low energy electrons responsible for the jet's energy transport and for the highest energy electrons with  $\gamma \approx 10^7$  responsible for the knot X-ray emission. Thus one could reasonably expect to see a marked change in  $\alpha_x$  moving from knot to inter-knot regions.

The largest hurdle for the application of synchrotron emission to jets of quasars comes from those cases for which the optical intensity is so low (or undetected) that it precludes a concave downward spectral fit from radio to X-rays. The associated 'bow-tie' problem (sec. 1.4) has been reported also for FRI sources (e.g. 3C120, knot 'k25' Harris, Mossman & Walker 2004). None of the possible solutions has been accepted by the community and progress on this issue depends on a demonstration that a key ingredient of spectral hardening at high energy is indicated by some independent means. Examples would be the confirmation of a prediction from the two-zone model or finding independent support for the shear layer acceleration model.

## 4.2 Critique of the IC/CMB Emission Model

The idea of augmenting  $u(\nu)$  compared to  $u(B)$  in the jet frame had been used for jets close to black holes where  $u(\nu)$  was thought to be dominated by UV radiation (e.g. Blandford & Levinson 1995, Dermer & Schlickeiser 1994, Sikora et al. 1997). Celotti, Ghisellini & Chiaberge (2001) and Tavecchio et al. (2000) applied this concept to kpc scale jets for which the CMB dominates  $u(\nu)$ . By positing that the X-ray knots of PKS0637-752 had a value of  $\Gamma \approx 10$ , similar to the values deduced from superluminal proper motions for the pc scale jet (Tingay et al. 2000), they were able to show that IC/CMB was able to explain the observed X-ray intensities while still maintaining equipartition conditions between  $u(B)$  and  $u(p)$  (where  $u(p)$  is the energy density in relativistic particles). This idea was quickly adopted by the community because it was already realized that the preponderance of one-sided X-ray jets requires  $\Gamma \geq 3$  or 4 and it provided a solution to the vexing problem of too little optical intensity to provide a reasonable synchrotron fit to the spectrum.

Additional support for this model is supplied by the jets that show the progression, discussed above, with a decreasing ratio of X-ray to radio intensity moving away from the core. Under the IC/CMB model, all that is required is a general deceleration of the jet, thereby reducing  $u'(\nu)$  in the jet frame (e.g. for 3C273, Sambruna et al. 2001). There is, of course the problem of explaining why the IC/CMB X-ray intensity of 3C273/knot A happens to fall so close to the extrapolation of the radio/optical synchrotron spectrum (Marshall et al. 2001).

There are a number of additional uncertainties and problems for the IC/CMB model although none of these represents a definitive refutation.

**Offsets and lifetime considerations** In sec. 3.2.1 we discussed offsets between X-ray and radio brightness distributions of jet knots. The low energy ( $\gamma \approx 100$ ) electrons responsible for the X-ray emission will have  $E^2$  lifetimes in excess of  $10^6$  yr; sufficient to travel to the end of even a Mpc jet. Thus when confronted with a knotty X-ray jet, the question arises: once a copious supply of these electrons are generated (e.g. at knot A in 3C273), why does the emission fade to a low level and then rise again for the next knot instead of forming a continuous or cumulatively brightening jet? One might devise a rather contrived

scenario by having the beaming factor decrease to end one knot, and then either increase at the location of the next knot, or posit the injection of enough new electrons to produce a bright knot, even if the beaming factor were smaller than that of the first knot. This explanation is unsatisfactory when the radio emission is considered since it should follow the X-ray behavior if  $\delta$  is the controlling factor. The same sort of problem affects the observed offsets (Atoyan & Dermer 2004, Stawarz et al. 2004); the X-ray brightness should persist further downstream than the optical and radio, the opposite of what is observed.

**Energetics** Atoyan & Dermer (2004), Dermer & Atoyan (2004) have made a comprehensive review of the X-ray emission processes and emphasize that the original formulation of IC/CMB emission worked on the equipartition assumption based on the radio data. When the electron spectrum is extended down to the low energies required by IC/CMB, the particle energy density [and hence also  $u(B)$ ] increase significantly. This leads them to conclude that excessive energies for the jet are required, even under the “optimistic” assumption that the jet is made of an electron/positron plasma without cold protons. For PKS0637-752, they find the kinetic luminosity is  $\geq 7 \times 10^{46}$  erg s<sup>-1</sup> for  $\delta=27$ ,  $\theta \leq 2^\circ$ , and increases for more reasonable beaming parameters. The associated total energy is  $\geq 10^{57}$  ergs for the case of  $\delta = \Gamma \approx 10$ ,  $\theta \approx 5^\circ$ .

**Uncertainty of extrapolation of the electron spectrum** One of the implicit assumptions of every IC/CMB calculation (i.e. to determine the required beaming parameters to explain the observed radio and X-ray intensities) is that the electron spectrum extends to very low energies with a slope  $p=2\alpha_r+1$ . If that were to be the case, then  $\alpha_x$  should have the same value as  $\alpha_r$ . However, as demonstrated in fig. 5, we currently have no knowledge that this condition holds. If  $\alpha_x$  is less than  $\alpha_r$ , it would indicate a low frequency break to a flatter spectrum and the estimated beaming parameters would be wrong. With fewer low energy electrons than assumed by the extrapolation,  $\Gamma$  and  $\delta$  would have to be larger and  $\theta$  correspondingly smaller, exacerbating some of the problems listed above. It is, of course, conceivable that the electron spectrum takes an upturn at low energies, in which case the error goes in the opposite direction.

Another assumption often, but not always present is that of equipartition. Since every calculation requires a value of the magnetic field in order to move from the observed segment of the synchrotron spectrum to obtain the corresponding segment of the electron spectrum, the usual method is to assume equipartition. When that constraint is removed as in the case of arguing for a field strength well below equipartition (e.g. Kataoka & Stawarz 2005), the electron spectrum can be considered to be undefined and one can conjure up whatever number of low energy electrons are needed to explain the X-rays for a given beaming factor. In the case of Kataoka & Stawarz (2005), a small value of  $\Gamma$  was invoked based on radio asymmetry arguments (Wardle & Aaron 1997). The initial analysis of PKS0637-752 (Schwartz et al. 2000) also suggested substantial dominance of  $u(p)$  since the IC/CMB scenario with beaming was not widely known at that time.

Finally, not only do IC/CMB models require a substantial extrapolation of the electron energy distribution to low energies with a fixed power law, they also require some fine tuning of a strict cutoff in the distribution at some slightly lower  $\gamma$  in order not to over-produce the optical emission (e.g. Sambruna et al.

2004, Table 7).

**Small angles to the line of sight and physical length of jets** From recent quasar surveys with the CXO (Marshall et al. 2005, Sambruna et al. 2004, Schwartz et al. 2006), fitting IC/CMB models yield  $\delta$  values which range from 3 to 11. For  $\Gamma = \delta$ , this means  $\theta$  is most commonly between  $4^\circ$  and  $11^\circ$ . Since most X-ray jets are reasonably straight, the physical length of jets sometimes exceeds 1 Mpc (n.b. the jet lengths given in Tables 1 and 2 refer primarily to the X-ray extent; the radio jet is often longer).

Many workers (e.g. Dermer & Atoyan 2004) find Mpc scale quasar jets uncomfortably long, and it is certainly the case that most FRII radio galaxies, the 'face-on' counterparts of quasars under the unified scheme, are much smaller. However, there are a small number of 'giant radio galaxies', and even a few quasars with sizes considerably greater than 1 Mpc (e.g. Riley & Warner 1990).

In some cases source morphology inferences are in conflict with small  $\theta$ . Wilson, Young & Shopbell (2001) argue that if the IC/CMB model with equipartition is applied to the jet in Pictor A,  $\Gamma = \delta = 7.2$  and  $\theta = 8^\circ$ . Such an angle to the line of sight would mean that the total extent of the source would be on the order of 3 Mpc and the hotspots at the outer end of each lobe, should be seen projected onto the radio lobes instead of protruding beyond the lobes as they are actually situated. Although Wilson, Young & Shopbell (2001) conclude that an IC/CMB model at a more reasonable  $\theta \approx 23^\circ$  would require  $B < B_{eq}$ , Hardcastle & Croston (2005) subsequently have made a strong case that the X-ray emission from the Pictor A jet is synchrotron emission, not IC/CMB.

**Expectations for jets with  $z > 1$**  Schwartz (2002) has argued that at higher redshifts there should be more jet detections since the increase in  $u(\nu)$  of the CMB by the factor  $(1+z)^4$  will compensate for the usual redshift dimming of surface brightness. In addition to this effect, we might expect to see more of the lower  $\Gamma$  jets with larger beaming cones because the  $(1+z)^4$  factor already will statistically increase the ratio of  $u(\nu)/u(B)$  regardless of the  $\Gamma^2$  factor from the jet's bulk velocity. So far, these predictions have not been realized (Bassett et al. 2004), and Kataoka & Stawarz (2005, see their fig. 10) have emphasized that the required  $\delta$  values for the IC/CMB model generally decrease with redshift. At this stage, the only quasar jet detection with  $z$  substantially  $\geq 2$  is GB 1508+5714 ( $z=4.3$ ).

### 4.3 Tests to differentiate between synchrotron and IC/CMB models

The basic tenet of the IC/CMB model for jet knots is that the X-ray emission is sampling the low energy end of the power law electron distribution. Therefore, the IC emission must continue to higher frequencies, unlike the synchrotron spectrum which is already relatively steep, and most likely will show an exponential cutoff at somewhat harder X-ray energies than available with the CXO. If we could measure the X-ray spectrum of quasar knots at much higher frequencies, and found a smooth continuation, it would be a clear confirmation of the IC/CMB model. If on the other hand, we were to find a cutoff in the X-ray spectrum, that would indicate synchrotron emission. Unfortunately, there are no real prospects of convincingly performing this test since it is so difficult to reach the required

sensitivity and angular resolution above 10 keV. The CXO band is too narrow to define the expected cutoff which may well be smeared over a wide frequency band by internal source structure.

Another option for discriminating these emission mechanisms will become available as new radio telescopes with unprecedented sensitivity and resolution at low frequencies come on line in the next few years. Both LOFAR in the Netherlands and the LWA (Long Wavelength Array) in the US will have the capability to resolve jet knots and determine the characteristics of the electron distribution at the low energies of interest (fig. 5). Each of these instruments will have a reasonably wide frequency coverage so that not only the amplitude, but also the slope of the low frequency emission can be measured. If we find that the low frequency radio data indicates that the spectrum flattens significantly or has a low frequency cutoff, then the IC/CMB model will have serious problems.

Optical and IR telescopes can be used to achieve detections of jet knots which currently have only upper limits. This band plays a crucial role for the IC/CMB model because there is still substantial uncertainty as to the origin of the currently detected optical features: is this emission from the top end of the synchrotron spectrum or the bottom end of the IC spectrum? Robust detections and photometry at several wavelengths should clarify this problem which impacts on the general 'fine tuning' of the low energy end of the electron spectrum (sec. 4.2).

#### 4.4 Detectability of the Extended Jet Emission By Gamma-Ray Telescopes

The *EGRET* detector on board the Compton Gamma-Ray Observatory established that blazars, AGNs with their jets aligned with the line of sight, are strong sources of gamma-rays. The EGRET experiment (approximately 20 MeV to 30 GeV, or  $5 \times 10^{21}$  to  $7 \times 10^{24}$  Hz) detected a total of 66 blazars with redshifts up to  $z \sim 2$  (Hartman, Bertsch & Bloom 1999). A small number of blazars (currently 10) with redshifts between 0.031 and 0.186 have been detected at even higher energies (GeV to TeV, frequencies above  $10^{25}$  Hz) with ground-based Cherenkov telescopes (Krawczynski 2005). Rapid gamma-ray flux variability on time scales between 15 min and a few hours, together with assumptions about infrared to UV emission co-spatially emitted with the gamma-rays, have been used to derive a lower limit on the Doppler factor  $\delta \gtrsim 10$  of the emitting plasma based on gamma-ray opacity arguments (Gaidos et al. 1996; Mattox, Wagner & Malkan 1997). All of these observations refer to very small physical scales, resulting in completely unresolved data from the nuclear regions.

If the extended jet emission detected by Chandra indeed originates from the IC/CMB process, the IC component should in principle be detectable in the MeV/GeV energy range with the Gamma-ray Large Area Space Telescope (GLAST) to be launched in 2007 (McEnery, Moskalenko & Ormes 2004), and possibly also in the GeV/TeV energy regime with ground-based telescopes like H.E.S.S., VERITAS, MAGIC, and CANGAROO III (Aharonian 2004, Weekes 2003). GLAST has a sensitivity for the flux above 100 MeV of  $3 \times 10^{-13}$  ergs  $\text{cm}^{-2}\text{s}^{-1}$  for 5 yrs of sky-survey observations. Cherenkov telescopes like VERITAS and H.E.S.S. have a 100 GeV sensitivity of  $9 \times 10^{-13}$  ergs  $\text{cm}^{-2}\text{s}^{-1}$  for 100hrs integration. These estimates have been derived by the instrument teams for photon indices of 2. For harder photon spectra with indices of 1.5, the  $\nu \times f_\nu$  sensitivities are about a factor of 2 better. IC/CMB models predict gamma-ray fluxes between  $10^{-13}$  and



a few times  $10^{-12}$  ergs  $\text{cm}^{-2}$   $\text{s}^{-1}$  (Dermer & Atoyan 2004, Tavecchio et al. 2004) so these new observatories should have sufficient sensitivity for detection.

The angular resolution of GLAST for a single photon will be  $3.4^\circ$  at 100 MeV, and  $0.1^\circ$  at 10 GeV; typical source localization accuracies will be tens of arcminutes near detection threshold and 0.5 arcmin for very strong sources<sup>5</sup>. For most sources, the angular distance between the core and kpc-scale jet is only a few arcsec, and GLAST will not be able to distinguish between core and jet emission on the basis of the spatial information. Furthermore, variability studies will be limited to rather long time scales and large fractional flux variations.

Cherenkov telescopes have better angular resolutions ( $\approx 0.1^\circ$ ) and source localization accuracies ( $\approx 20''$ ). For  $\sim 100$  GeV photons however, the transparency of the Universe is limited to redshifts on the order of 0.5 owing to the gamma-rays pair-producing on IR background photons (1 to 40 microns) from galaxies. Detection and identification of gamma-rays from kpc-scale jets would thus require very strong sources with very extended X-ray jets at low redshifts; the chances for obtaining unambiguous results are not promising.

## 4.5 Prospects

**4.5.1 SYNCHROTRON EMISSION** In general, synchrotron emission is a powerful diagnostic of relativistic plasmas, and in the particular case of X-ray frequencies, informs us as to the location of acceleration sites. The major problem is the unknown magnetic field strength which precludes a direct determination of the electron energy distribution.

Since the X-ray emitting electrons have such a high energy and consequently short lifetime, we expect variability in jets will continue to offer new insights. With a multifrequency monitoring, it should be possible to disentangle light travel times from  $E^2$  halflives and thus obtain a different estimate of the magnetic field strength and or  $u'(\nu)$  as well as  $\delta$  (Harris et al. 2006).

As more jets are studied with greater sensitivity, we believe the chances are good that we should find a few objects that display the effects of a high energy cutoff in the CXO band. Though we assume that all synchrotron plasmas have cutoffs, few if any have actually been observed in radio, optical, or X-rays. This result would impact the acceleration scenario by providing an estimate of the extent in energy of the electron distribution.

On the theoretical front, we need additional ideas of how deviations from a power law electron spectrum can occur. The two proposals currently available are rather restricted in applicability and should be further developed.

**4.5.2 IC EMISSION** If the jet X-ray emission from powerful sources is indeed from the IC/CMB process, we can study different attributes of the underlying relativistic plasma than those involved in synchrotron emission. In particular, we can obtain vital information about the low energy part of the electron spectrum. Both the amplitude and slope for  $\gamma \leq 1000$  are germane to the injection problem for shock acceleration as well as permitting greatly improved estimates of the total particle energy density and hence the energetics of the emitting plasma.

As is well known, estimates of the photon energy density are amenable to direct observational input, and this permits us to pass more confidently from the emission spectrum to the electron spectrum. Once the electron spectrum is

<sup>5</sup><http://www-glast.slac.stanford.edu/>

known, then the observed synchrotron component will provide the magnetic field strength. The basic physics is understood and IC emission is mandatory in all relativistic plasmas. The only questions are, how much emission is there and what is the frequency range of the emission.

For the beaming IC/CMB model applied to jets, some 'paradigm shifts' will be in order. If current estimates of beaming parameters are correct, many of the relatively bright X-ray knots are, in their own frame, rather unimpressive: luminosities of order  $10^{38}$  to  $10^{39}$  erg s<sup>-1</sup> would be common and the canonical  $10^{44}$  erg s<sup>-1</sup> would no longer be relevant.

Another effect means that our view of jets close to the line of sight is actually a stretched out version of the time history of a very small fraction of the 'current jet length' (by which we mean the distance from the outermost knot or hotspot to the core, at the time we observe the jet tip). This can be quickly grasped by reversing time and sending a signal from the earth to the quasar. As the wavefront of our signal passes the jet tip, the jet is moving relativistically towards the quasar. For example, take a 100,000 l.y. jet at 5° to our line of sight. If the jet has a bulk velocity of 0.99c, by the time our wavefront reaches the quasar about 98.6% of the jet (as it existed when our wavefront first reached the tip) has now been swallowed by the black hole, and is thus not observable by us. What we see, which appears to be 100,000 l.y. in length, is actually just the 1,400 l.y. long tip of the 'current jet', as it was at progressively earlier times as we move back from the tip. The most important aspect of this effect is to make the necessary adjustments when comparing quasar jets to those lying closer to the plane of the sky. What might we actually be studying if all we see is 1% of the 'current jet length'? The hotspot? If so, what we call knots in the jets would actually be bits of the hotspot brightening and fading over its 100,000 year long journey to its 'present' location.

## 4.6 Summary

Within a few years, the uncertainty as to the X-ray emission process for quasar jets should be eliminated and then we will either have a method of measuring the low energy end of the relativistic electron distribution (if the IC/CMB model applies) or we will have new insights into the behavior and loss mechanisms affecting the highest energy electrons (if synchrotron models apply). If we are convinced that the IC/CMB model is correct, then a number of conclusions are already clear: detected quasar jets lie close to the line of sight and have large Lorentz factors. That in turn means we can solve for some of the basic jet parameters such as energy flux, and most likely we will improve our understanding of cross-jet velocity structure: many different lines of argument point to the necessity of some sort of 'spine-sheath' structure.

In part 2 of this review, we have examined the differences between the jets of FRI radio galaxies and those of quasars. Will the distinctions in jet length and luminosity translate to differences in X-ray emission process? If so, why are there so many similarities between low power and high power sources such as offsets and progressions? We may also expect to better understand the underlying reasons for brightness fluctuations along jets, and if the small knots of FRI jets have the same genesis as the kpc scale knots in quasar jets. All of these lines of investigation will hopefully elucidate the dichotomy between the plasma that emits the radiation we observe and the medium which transports the energy and

momentum over such vast distances.

## 5 ACKNOWLEDGMENTS

We thank C. Cheung, S. Jester, M. Hardcastle, and many other colleagues for useful discussions. C. Cheung, and L. Stawarz kindly gave us helpful comments on the manuscript and the editor, R. Blandford, provided valuable advice. This work has made use of NASA's Astrophysics Data System Bibliographic Services and the XJET website. Partial support was provided by NASA contract NAS8-03060 and grant GO3-4124A. HK thanks the Department of Energy for support in the framework of the Outstanding Junior Investigator program.

## References

- Aharonian FA. 2002. *MNRAS* 332:215–230
- Aharonian FA. 2004. *Very high energy cosmic gamma radiation: a crucial window on the extreme universe*. River Edge, NJ: World Scientific Publishing
- Aldcroft T, Siemiginowska A, Elvis M, Mathur S, Nicastro F, Murray S. 2003. *ApJ* 597:751
- Atoyan A, Dermer CD. 2004. *ApJ* 613:151–158
- Bahcall JN, Kirhakos S, Schneider DP, Davis RJ, Muxlow TWB, et al. 1995. *ApJL* 452:L91
- Bai JM, Lee MG. 2003. *ApJL* 585:L113–L116
- Bassett LC, Brandt WN, Schneider DP, Vignali C, Chartas G, Garmire GP. 2004. *A.J.* 128:523–533
- Begelman MC, Blandford RD, Rees MJ. 1984. *RvMP* 56:255
- Bell AR. 1978. *MNRAS* 182:147
- Beresnyak AR, Istomin YN, Pariev VI. 2003. *Astron. & Astrophys.* 403:793–804
- Bicknell GV. 1995. *ApJ Suppl.* 101:29
- Bicknell GV, Begelman MC. 1996. *ApJ* 467:597
- Biretta JA, Sparks WB, Macchetto F. 1999. *ApJ* 520:621
- Birkinshaw M, Worrall DM, Hardcastle MJ. 2002. *MNRAS* 335:142–150
- Blandford R, Payne DG. 1982. *MNRAS* 199:883
- Blandford R, Rees M. 1974. *MNRAS* 169:395
- Blandford RD. 1976. *MNRAS* 176:465–481
- Blandford RD, Levinson A. 1995. *ApJ* 441:79
- Blandford RD, Ostriker JP. 1978. *ApJ* 221:L29
- Blandford RD, Znajek RL. 1977. *MNRAS* 179:433–456
- Bodo G, Rossi P, Mignone A, Massaglia S, Ferrari A. 2003. *New Astronomy Review* 47:557–559
- Bridle AH, Hough DH, Lonsdale CJ, Burns JO, Laing RA. 1994. *A.J.* 108:766–820
- Brunetti G, Harris D, Sambruna R, Setti G. 2003. *NewAR* 47:411–712
- Celotti A, Fabian AC. 1993. *MNRAS* 264:228
- Celotti A, Ghisellini G, Chiaberge M. 2001. *MNRAS* 321:L1–L5
- Chartas G, Gupta V, Garmire G, Jones C, Falco EE, et al. 2002. *ApJ* 565:96–104

- Chartas G, Worrall DM, Birkinshaw M, Cresitello-Dittmar M, Cui W, et al. 2000. *ApJ* 542:655–666
- Cheung CC. 2004. *ApJL* 600:L23–L26
- Chiaberge M, Celotti A, Capetti A, Ghisellini G. 2000. *Astron. & Astrophys.* 358:104–112
- Chiaberge M, Gilli R, Macchetto F, Sparks W, Capetti A. 2003. *ApJ* 582:645
- Comastri A, Brunetti G, Dallacasa D, Bondi M, Pedani M, Setti G. 2003. *MNRAS* 340:L52
- Coppi PS. 1999. In *Relativistic Jets in AGNs*, eds. M Ostrowski, M Sikora, G Madejski, M Begelman. Jagellonian University Press. Astro-ph/9903162
- Curtis HD. 1918. *Pub. Lick. Obs.* 13:31
- Dennett-Thorpe J, Bridle A, Scheuer P, Laing R, Leahy J. 1997. *MNRAS* 289:753
- Dermer CD, Atoyan A. 2004. *ApJ* 611:L9
- Dermer CD, Atoyan AM. 2002. *ApJL* 568:L81–L84
- Dermer CD, Schlickeiser R. 1994. *ApJ Suppl.* 90:945–948
- Evans DA, Hardcastle MJ, Croston JH, Worrall DM, Birkinshaw M. 2005. *MNRAS* 359:363–382
- Fabian A, Celotti A, Johnstone R. 2003. *MNRAS* 338:L7
- Fukue J, Tojyo M, Hirai Y. 2001. *Pub. Ast. Soc. Japan* 53:555–563
- Gabuzda DC, Murray É, Cronin P. 2004. *MNRAS* 351:L89–L93
- Gaidos JA, Akerlof CW, Biller SD, et al. 1996. *Nature* 383:319
- Georganopoulos M, Kazanas D. 2003. *ApJL* 589:L5–L8
- Georganopoulos M, Kazanas D. 2004. *ApJL* 604:L81–L84
- Ghisellini G, Tavecchio F, Chiaberge M. 2005. *Astron. & Astrophys.* 432:401–410
- Graziani C, Lamb DQ, Donaghy TQ. 2006. *ApJ* submitted [astro-ph/0505623]
- Hardcastle M, Birkinshaw M, Worrall D. 2001. *MNRAS* 326:1499
- Hardcastle M, Croston J. 2005. *MNRAS* 363:649
- Hardcastle MJ, Harris DE, Worrall DM, Birkinshaw M. 2004a. *ApJ* 612:729–748
- Hardcastle MJ, Worrall DM, Birkinshaw M, Laing RA, Bridle AH. 2002. *MNRAS* 334:182–192
- Hardcastle MJ, Worrall DM, Birkinshaw M, Laing RA, Bridle AH. 2005. *MNRAS* 358:843–850
- Hardcastle MJ, Worrall DM, Kraft RP, Forman WR, Jones C, Murray SS. 2003. *ApJ* 593:169–183
- Hardcastle MJ, Worrall DM, Kraft RP, Forman WR, Jones C, Murray SS. 2004b. *Nuclear Physics B Proceedings Supplements* 132:116–121
- Hardee PE, Walker RC, Gómez JL. 2005. *ApJ* 620:646–664
- Harris D, Mossman A, Walker R. 2004. *ApJ* 615:161
- Harris DE, Carilli CL, Perley RA. 1994. *Nature* 367:713
- Harris DE, Cheung CC, Biretta JA, Junor W, Perlman ES, et al. 2006. *ApJ* 640:211
- Harris DE, Finoguenov A, Bridle AH, Hardcastle MJ, Laing RA. 2002. *ApJ* 580:110–113
- Harris DE, Hjorth J, Sadun AC, Silverman JD, Vestergaard M. 1999. *ApJ* 518:213–218
- Harris DE, Krawczynski H. 2002. *ApJ* 565:244–255

- Harris DE, Krawczynski H. 2006. In *Triggering Relativistic Jets*, eds. W Lee, E Ramirez-Ruiz, vol. in press of *Revista Mexicana de Astronomia y Astrofisica, Serie de Conferencias*
- Harris DE, Krawczynski H, Taylor GB. 2002. *ApJ* 578:60–63
- Hartman RC, Bertsch DL, Bloom SD. 1999. *ApJ Suppl.* 123:79
- Hirofani K, Iguchi S, Kimura M, Wajima K. 1999. *Pub. Ast. Soc. Japan* 51:263–267
- Hughes PA. 1991. *Beams and jets in astrophysics*. Press Syndicate of the Univ. of Cambridge, Cambridge University Press, Cambridge
- Jester S, Harris DE, Marshall H, Meisenheimer K, Perley R. 2006. *ApJ* in press
- Jester S, Röser HJ, Meisenheimer K, Perley R. 2005. *Astron. & Astrophys.* 431:477–502
- Jorstad SG, Marscher AP. 2004. *ApJ* 614:615–625
- Jorstad SG, Marscher AP, Lister ML, Stirling AM, Cawthorne TV, et al. 2005. *A.J.* 130:1418–1465
- Kataoka J, Edwards P, Georganopoulos M, Takahara F, Wagner S. 2003. *A&A* 399:91
- Kataoka J, Stawarz L. 2005. *ApJ* 622:797–810
- Kataoka J, Stawarz L, Aharonian F, Takahara F, Ostrowski M, Edwards PG. 2006. *ApJ* submitted:astro-ph 05100661
- Kellermann KI, Lister ML, Homan DC, Vermeulen RC, Cohen MH, et al. 2004. *ApJ* 609:539–563
- Kino M, Takahara F, Kusunose M. 2002. *ApJ* 564:97
- Kirk JG, Duffy P. 1999. *J. Phys. G.* 25:163
- Koide S, Shibata K, Kudoh T. 1999. *ApJ* 522:727
- Komissarov SS. 1994. *MNRAS* 266:649
- Königl A. 1980. *Relativistic Effects in Extragalactic Radio Sources*. Ph.D. thesis, California Institute of Technology, Pasadena, CA
- Kraft RP, Forman WR, Jones C, Murray SS, Hardcastle MJ, Worrall DM. 2002. *ApJ* 569:54–71
- Kraft RP, Hardcastle MJ, Worrall DM, Murray SS. 2005. *ApJ* 622:149–159
- Krawczynski H. 2004. *NewAR* 48:367
- Krawczynski H. 2005. *AIP Proc.* in press, [astro-ph 050862]
- Krawczynski H, Coppi PS, Aharonian FA. 2002. *MNRAS* 336:721
- Laing RA, Bridle AH. 2002a. *MNRAS* 336:1161–1180
- Laing RA, Bridle AH. 2002b. *MNRAS* 336:328–352
- Laing RA, Bridle AH. 2004. *MNRAS* 348:1459–1472
- Laing RA, Canvin JR, Bridle AH. 2003. *New Astronomy Review* 47:577–579
- Lara L, Giovannini G, Cotton WD, Feretti L, Venturi T. 2004. *Astron. & Astrophys.* 415:905–913
- Lee WH, Ramirez-Ruiz E, eds. 2006. vol. in press. *Revista Mexicana de Astronomia y Astrofisica, Serie de Conferencias*
- Lister ML. 2003. *ApJ* 599:105–115
- Lobanov A, Hardee P, Eilek J. 2003. *New Astronomy Review* 47:629–632
- Lovelace RVE. 1976. *Nature* 262:649–652
- Ly C, De Young DS, Bechtold J. 2005. *ApJ* 618:609–617



- Macchetto FD. 1996. In *IAU Symp. 175: Extragalactic Radio Sources*
- Marshall HL, Harris DE, Grimes JP, Drake JJ, Fruscione A, et al. 2001. *ApJL* 549:L167–L171
- Marshall HL, Miller BP, Davis DS, Perlman ES, Wise M, et al. 2002. *ApJ* 564:683–687
- Marshall HL, Schwartz DA, Lovell JEJ, Murphy DW, Worrall DM, et al. 2005. *ApJ Suppl.* 156:13–33
- Mattox JR, Wagner SJ, Malkan M. 1997. *ApJ* 476:692
- McEnery JE, Moskalenko IV, Ormes JF. 2004. In “*Cosmic Gamma Ray Sources*”, eds. K Cheng, G Romero. Kluwer ASSL Series. Astro-ph/0406250
- Nakamura M, Uchida Y, Hirose S. 2001. *New Astronomy* 6:61–78
- Nishikawa KI, Hardee P, Richardson G, Preece R, Sol H, Fishman GJ. 2005. *ApJ* 622:927
- Ostrowski M, Sikora M, Madejski G, Begelman M, eds. 1997. *Relativistic Jets in AGNs*, Konfederacka 6, 30-306, Krakow. Poligrafia Inspektoratu Towarzystwa Salezjanskiego
- Perlman ES, Harris DE, Biretta JA, Sparks WB, Macchetto FD. 2003. *ApJL* 599:L65–L68
- Perlman ES, Wilson AS. 2005. *ApJ* 627:140–155
- Pesce JE, Sambruna RM, Tavecchio F, Maraschi L, Cheung CC, et al. 2001. *ApJL* 556:L79–L82
- Pushkarev AB, Gabuzda DC, Vetukhnovskaya YN, Yakimov VE. 2005. *MNRAS* 356:859–871
- Rees MJ. 1971. *Nature* 229:312
- Riley JM, Warner PJ. 1990. *MNRAS* 246:1P
- Rossi P, Bodo G, Massaglia S, Ferrari A, Mignone A. 2004. *Ap&SS* 293:149–155
- Salpeter EE. 1964. *ApJ* 140:796–800
- Sambruna R, Urry C, Tavecchio F, Maraschi L, Scarpa R, et al. 2001. *ApJ* 549:L161
- Sambruna RM, Gambill JK, Maraschi L, Tavecchio F, Cerutti R, et al. 2004. *ApJ* 608:698–720
- Sambruna RM, Maraschi L, Tavecchio F, Urry CM, Cheung CC, et al. 2002. *ApJ* 571:206–217
- Sauty C, Tsinganos K, Trussoni E. 2002. *LNP Vol. 589: Relativistic Flows in Astrophysics* 589:41
- Scheuer P. 1974. *MNRAS* 166:513
- Schwartz DA. 2002. *ApJ* 569:L23
- Schwartz DA, Marshall HL, Lovell JEJ, Murphy DW, Bicknell GV, et al. 2006. *ApJ* in press:astro-ph 0601632
- Schwartz DA, Marshall HL, Lovell JEJ, Piner BG, Tingay SJ, et al. 2000. *ApJL* 540:L69
- Siemiginowska A, Bechtold J, Aldcroft TL, Elvis M, Harris DE, Dobrzycki A. 2002. *ApJ* 570:543–556
- Siemiginowska A, Smith RK, Aldcroft TL, Schwartz DA, Paerels F, Petric AO. 2003. *ApJL* 598:L15–L18
- Siemiginowska A, Stanghellini C, Brunetti G, Fiore F, Aldcroft T, et al. 2003. *ApJ* 595:643
- Sikora M, Begelman MC, Madejski GM, Lasota JP. 2005. *ApJ* 625:72–77
- Sikora M, Madejski G. 2001. *AIP* 558:275

- Sikora M, Madejski G, Moderski R, Poutanen J. 1997. *ApJ* 484:108
- Spada M, Ghisellini G, Lazzati D, Celotti A. 2001. *MNRAS* 325:1559–1570
- Stawarz L. 2004. *ApJ* 613:119–128
- Stawarz L, Ostrowski M. 2002. *ApJ* 578:763–774
- Stawarz L, Sikora M, Ostrowski M, Begelman MC. 2004. *ApJ* 608:95–107
- Swain MR, Bridle AH, Baum SA. 1998. *ApJL* 507:L29–L33
- Tanihata C, Takahashi T, Kataoka J, Madejski GM. 2003. *ApJ* 584:153
- Tavecchio F. 2004. *Memorie della Societa Astronomica Italiana Supplement* 5:211
- Tavecchio F. 2005. In *Procs. the X'th Marcel Grossmann Meeting on General Relativity, Rio de Janeiro, Brazil, July 2003*, vol. astro-ph/0401590
- Tavecchio F, Maraschi L, Sambruna RM, et al. 2004. *ApJ* 614:64
- Tavecchio F, Maraschi L, Sambruna RM, Urry CM. 2000. *ApJL* 544:L23–L26
- Tingay SJ, Jauncey DL, Reynolds JE, Tzioumis AK, King EA, et al. 2000. *Advances in Space Research* 26:677–680
- Tsiganos K, Bogovalov S. 2002. *MNRAS* 337:553–558
- Urry CM, Padovani P. 1995. *PASP* 107:803
- Uttley P, McHardy IM, Vaughan S. 2005. *MNRAS* 359:345
- Walker R, Benson J, Unwin S. 1987. *ApJ* 316:546
- Wang JC. 2002. *Chinese Journal of Astronomy and Astrophysics* 2:1–7
- Wardle JFC, Aaron SE. 1997. *MNRAS* 286:425
- Wardle JFC, Homan DC, Ojha R, Roberts DH. 1998. *Nature* 395:457–461
- Weekes T. 2003. *Very high energy gamma-ray astronomy*. The Institute of Physics Pub., Bristol, UK
- Weisskopf MC, Aldcroft TL, Bautz M, Cameron RA, Dewey D, et al. 2003. *Exper.Astron.* 16:1–68
- Wilson A, Young A, Shopbell P. 2001. *ApJ* 547:740
- Wilson AS, Yang Y. 2002. *ApJ* 568:133
- Worrall D, Birkinshaw M. 2005. *MNRAS* 360:926
- Worrall D, Birkinshaw M, Hardcastle M. 2001. *MNRAS* 326:L7
- Worrall DM, Birkinshaw M, Hardcastle MJ. 2003. *MNRAS* 343:L73–L78
- Zensus JA. 1997. *Ann. Rev. Ast. & Astrophys.* 35:607–636
- Zezas A, Birkinshaw M, Worrall DM, Peters A, Fabbiano G. 2005. *ApJ* 627:711–720

\*

Figure 2: A radio image of the quasar 3C351 at 1.4 GHz from the VLA. X-ray contours are superposed from CXO data. Contour levels increase by factors of 2, from 2 to 32 in arbitrary brightness units. Note the bright NE hotspot pair and the very weak S hotspot.

Figure 3: M87 CXO image with 8 GHz contours. The X-ray image has an effective exposure of about 115 ks, consisting of 22 observations taken between 2000 and 2004. It has been smoothed with a Gaussian of FWHM=0.25'' and the energy band is 0.2-6 keV. The color mapping is logarithmic and ranges from 0.02 (faint green) to a peak of 5.5  $\text{eV s}^{-1}$  ( $0.049'' \text{ pixel}^{-1}$ ) $^{-1}$ . The radio data are from the VLA with a beam of FWHM=0.2''. Contour levels increase by factors of 2 and start at 1 mJy/beam.

Table 1: Parameters for Jets of Low Power Radio Galaxies

| Host name     | z      | Scale<br>(kpc/'') | Length<br>(arcsec) | Length<br>(kpc) | log $L_x$<br>( $\text{ergs}^{-1}$ ) | $\alpha_x$   | $\theta$<br>(deg) | Deproj.<br>(kpc) | Reference |
|---------------|--------|-------------------|--------------------|-----------------|-------------------------------------|--------------|-------------------|------------------|-----------|
| 3C15*         | 0.0730 | 1.4               | 4                  | 5.6             | 41.03                               | 0.7±0.4      | ..                | ..               | 1         |
| NGC 315       | 0.0165 | 0.33              | 13                 | 4.3             | 40.54                               | 1.5±0.7      | ..                | ..               | 2         |
| 3C31*         | 0.0167 | 0.34              | 8                  | 2.7             | 40.56                               | 1.1±0.2      | 52                | 3.4              | 3         |
| B2 0206+35    | 0.0369 | 0.72              | 2                  | 1.4             | 41.12                               | ..           | ..                | ..               | 4         |
| 3C 66B*       | 0.0215 | 0.43              | 7                  | 3.0             | 41.03                               | 1.3±0.1      | ..                | ..               | 5         |
| 3C 120*       | 0.0330 | 0.65              | 80                 | 52              | 41.95                               | ..           | ..                | ..               | 6         |
| 3C 129        | 0.0208 | 0.42              | 2.5                | 1.0             | 39.64                               | ..           | ..                | ..               | 7         |
| PKS 0521-365* | 0.055  | 1.06              | 2                  | 2.1             | 41.90                               | 1.2±0.3      | ..                | ..               | 8         |
| B2 0755+37*   | 0.0428 | 0.83              | 4                  | 3.3             | 41.52                               | ..           | ..                | ..               | 4         |
| 3C270         | 0.0074 | 0.15              | 35                 | 5.2             | 39.13                               | ..           | ..                | ..               | 9, 10     |
| M84           | ...    | 0.082             | 3.9                | 0.3             | 38.71                               | 0.8±0.3      | 50                | 0.4              | 11        |
| M87*          | 0.0043 | 0.077             | 20                 | 1.5             | 41.32                               | >1           | 20                | 4.5              | 12, 13    |
| Cen A         | ...    | 0.017             | 120                | 2.0             | 39.39                               | 0.4 to 2.2   | 15                | 7.7              | 14        |
| Cen B         | 0.013  | 0.26              | 8                  | 2.1             | 40.13                               | ..           | ...               | ...              | 15        |
| 3C296         | 0.0237 | 0.47              | 10                 | 4.7             | 40.09                               | 1.0±0.4      | ..                | ..               | 16        |
| NGC6251*      | 0.0249 | 0.49              | 410                | 200             | ..                                  | 1.30±0.14    | ..                | ..               | 17        |
| 3C 346*       | 0.161  | 2.7               | 2                  | 5.4             | 41.96                               | 1.0±0.3      | 20                | 16               | 18        |
| 3C 371*       | 0.051  | 0.98              | 4                  | 3.9             | 41.87                               | 0.7+0.4,-0.2 | 18                | 12.6             | 19        |
| 3C 465        | 0.0293 | 0.58              | 7.5                | 4.4             | 40.30                               | ≈ 1.4        | ...               | ...              | 16        |

Notes

The scale is given in units of kpc per arcsec.

All sources are classified as FRI radio galaxies except for 3C120, a Seyfert I galaxy, and the two BL Lac objects, PKS0521-365 and 3C371.

A “\*” after the source name indicates that an optical detection has been reported, see <http://home.fnal.gov/~jester/optjets/>.

References

1 Kataoka et al. (2003); 2 Worrall, Birkinshaw & Hardcastle (2003); 3 Hardcastle et al. (2002); 4 Worrall, Birkinshaw & Hardcastle (2001); 5 Hardcastle, Birkinshaw & Worrall (2001); 6 Harris, Mossman & Walker (2004); 7 Harris, Krawczynski & Taylor (2002); 8 Birkinshaw, Worrall & Hardcastle (2002); 9 Zezas et al. (2005); 10 Chiaberge et al. (2003); 11 Harris et al. (2002); 12 Wilson & Yang (2002); 13 Marshall et al. (2002); 14 Hardcastle et al. (2003); 15 Marshall et al. (2005); 16 Hardcastle et al. (2005); 17 Evans et al. (2005); 18 Worrall & Birkinshaw (2005); 19 Pesce et al. (2001).

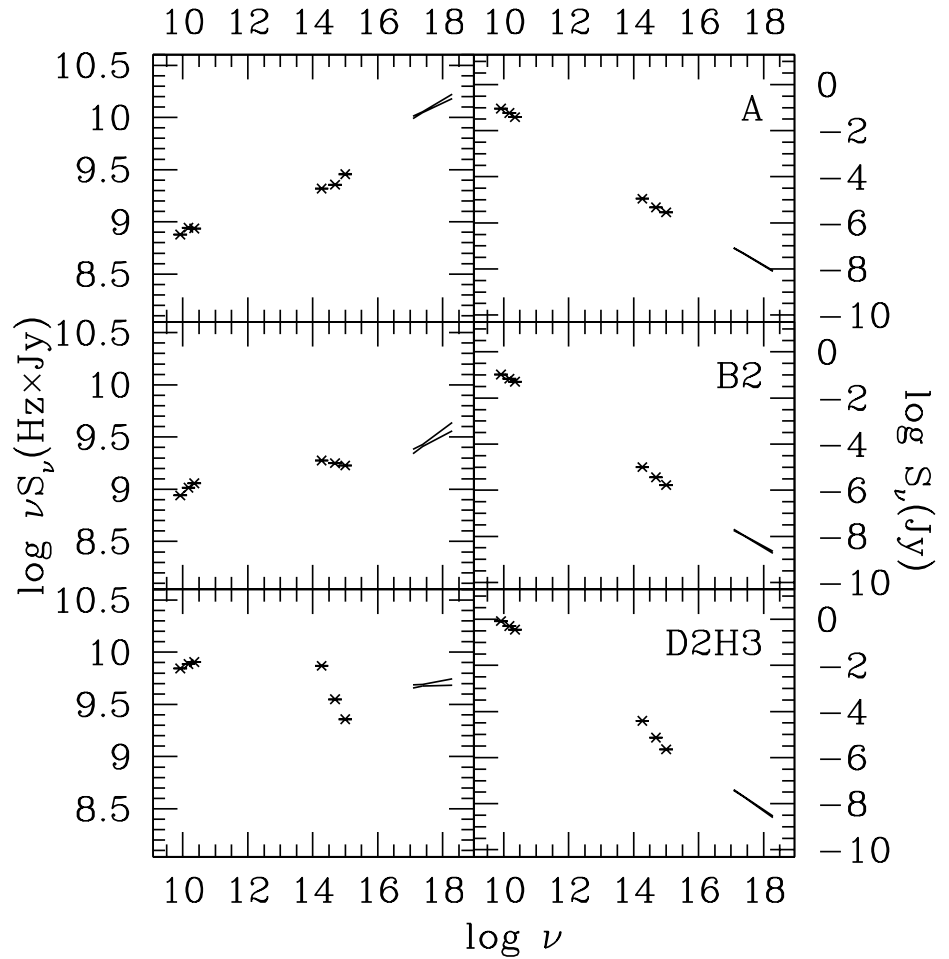


Figure 4: Examples of spectral energy distributions: 3 knots in the 3C273 jet. The left panels plot  $\log(\nu \times S_\nu)$  as ordinate and the right panels are versions with  $\log S_\nu$  vs.  $\log \nu$ . From top to bottom knots A, B2, and D2/H3 are shown. The X-ray data are presented as “bowties” which delineate the range of acceptable power-law slopes. Note how these data preclude a fit consisting of a single zone synchrotron spectrum which would be a curve concave downward. This figure was kindly provided by S. Jester. Details can be found in Jester et al. (2006).

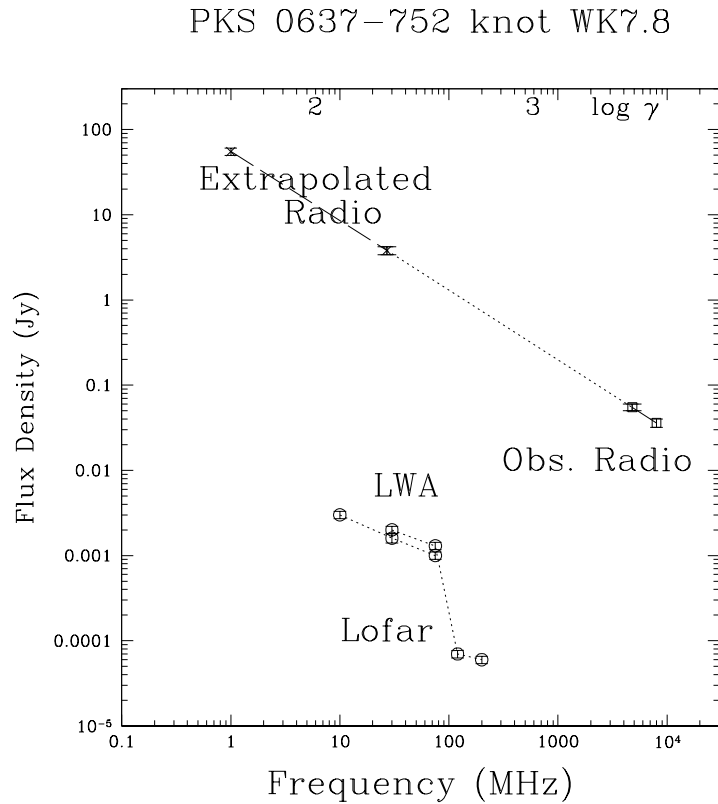


Figure 5: Segments of the synchrotron spectrum of knot WK7.8 in the jet of PKS0637-752. The observed radio flux densities are plotted toward the right edge so the short solid line allows us to determine a small section of the electron spectrum if we trust the equipartition field strength estimate; the extrapolation of this spectrum to lower frequencies is shown by the dotted line. The segment coming from the same electrons responsible for the IC/CMB X-ray emission is the long dash line to the upper left. Also shown near the bottom are sensitivity limits for low frequency radio telescopes being designed and under construction: LWA is the Long Wavelength Array planned for a site in the southwest of the US, and LOFAR is being built in the Netherlands. At the top are a few values of  $\log \gamma$  which indicates the energy of the electrons corresponding to the emission spectrum.



Figure 6: A comparison of 3 jets. The X-ray jets, M87 (top), 3C273 (middle), and PKS1127-145 (bottom) have been rotated for ease of comparison. All maps have had pixel randomization removed and have been smoothed with a Gaussian of FWHM=0.25". The absolute brightness mapping is logarithmic and the same for all three and ranges from 0.01 (pink) to 6.7 (the black peak of 3C273). The intensity units are total electron volts per sec per pixel and the pixel size is 0.0492". The overall projected size of each jet (from top to bottom) is 1.6, 56, and 238 kpc (21", 21", and 29", respectively). The small cyan line overlaid on the core of 3C273 shows the length of the M87 jet if it were moved to the distance of 3C273, and the cyan rectangle on the bottom panel represents the total length of the 3C273 jet if it were at the distance of PKS1127-145. The X-ray jet of PKS1127-145 is too faint to be visible on the common intensity scale adopted, so radio contours are overlaid in order to show the full extent of the jet. X-ray emission is detected out to the last radio feature (fig. 11).

Table 2: Parameters for Jets of High Power Radio Galaxies &amp; Quasars

| Host name     | z      | Scale<br>(kpc/as) | Length<br>(arcsec) | Length<br>(kpc) | log L <sub>x</sub><br>(ergs <sup>-1</sup> ) | α <sub>x</sub> | θ<br>(deg) | Deproj.<br>(kpc) | δ   | Reference |
|---------------|--------|-------------------|--------------------|-----------------|---|----------------|------------|------------------|-----|-----------|
| 3C9           | 2.012  | 8.5               | 6.4                | 54              | 44.34                                       | ..             | ..         | ..               | ..  | 1         |
| PKS 0208-512  | 0.999  | 8.04              | 5                  | 40              | 44.47                                       | ..             | 8          | 262              | 7   | 2,3       |
| PKS 0413-21   | 0.808  | 7.54              | 2                  | 15              | 43.99                                       | ..             | 20         | 44               | 3   | 2         |
| Pictor A      | 0.0350 | 0.69              | 114                | 79              | 40.84                                       | 0.97±0.07      | >23        | <201             | <3  | 4,5       |
| PKS 0605-085  | 0.870  | 7.7               | 4                  | 31              | 44.58                                       | 0.4±0.7        | ..         | ..               | ..  | 6         |
| PKS 0637-752* | 0.651  | 6.9               | 12                 | 83              | 44.34                                       | 0.85±0.08      | 5.7        | 836              | 10  | 7,8       |
| 3C 179        | 0.846  | 7.7               | 4.4                | 34              | 44.45                                       | ..             | ..         | ..               | ..  | 6         |
| B2 0738+313   | 0.635  | 6.9               | 35                 | 241             | 42.93                                       | 0.5 to 1.4     | 8          | 1730             | 7   | 9         |
| 0827+243      | 0.939  | 7.9               | 6.2                | 49              | 44.14                                       | 0.4±0.2        | 2.5        | 1100             | 20  | 10        |
| 3C 207        | 0.68   | 7.1               | 4.6                | 33              | 43.97                                       | 0.3±0.3        | 8          | 237              | 7   | 6         |
| 3C 212*       | 1.049  | 8.1               | 4                  | 32              | 43.52                                       | ..             | ..         | ..               | ..  | 11        |
| PKS 0903-57   | 0.695  | 7.1               | 3.5                | 25              | 43.90                                       | ..             | 20         | 73               | 3   | 2         |
| PKS 0920-39   | 0.591  | 6.6               | 10                 | 66              | 43.70                                       | ..             | 7          | 322              | 8   | 2,3       |
| 3C 219        | 0.174  | 2.9               | 20                 | 58              | (41.68)                                     | ..             | ..         | ..               | ..  | 12        |
| Q0957+561     | 1.41   | 8.5               | 8                  | 68              | 43.69                                       | 0.9±0.6        | ..         | ..               | 1.4 | 13        |
| PKS 1030-357  | 1.455  | 8.5               | 12                 | 102             | 44.99                                       | ..             | 8.6        | 682              | 9   | 2,3       |
| PKS 1046-40   | 0.620  | 6.8               | 4                  | 27              | 43.44                                       | ..             | 17         | 93               | 3   | 2         |
| PKS 1127-145  | 1.18   | 8.3               | 30                 | 249             | 44.62                                       | 0.5±0.2        | 24         | 612              | 4   | 14        |
| PKS 1136-135* | 0.554  | 6.4               | 6.7                | 43              | 43.92                                       | 0.4±0.4        | 6          | 410              | 10  | 6         |
| 4C49.22*      | 0.334  | 4.8               | 5.6                | 27              | 43.62                                       | ..             | 6          | 270              | 14  | 6         |
| PKS 1202-262  | 0.789  | 7.5               | 5                  | 37              | 44.73                                       | ..             | 4.9        | 568              | 12  | 2,3       |
| 3C 273*       | 0.1583 | 2.7               | 21                 | 57              | 43.58                                       | 0.6 to 0.9     | 5          | 654              | 5   | 16,17     |
| 4C19.44*      | 0.720  | 7.2               | 14.4               | 104             | 44.55                                       | ..             | 10         | 616              | 14  | 6         |
| 3C 303*       | 0.141  | 2.5               | 9                  | 22              | 41.56                                       | ..             | ..         | ..               | ..  | 17        |
| GB 1508+5714  | 4.3    | 6.9               | 2.2                | 15              | 44.96                                       | 0.9±0.4        | 15         | 58               | 4   | 18,21     |
| PKS 1510-089  | 0.361  | 5.0               | 5.2                | 26              | 43.85                                       | 0.5±0.4        | ..         | ..               | ..  | 6         |
| 3C 345*       | 0.594  | 6.6               | 2.7                | 18              | 43.65                                       | 0.7±0.9        | 7          | 138              | 7   | 6         |
| 1642+690      | 0.751  | 7.3               | 2.7                | 20              | 43.67                                       | ..             | ..         | ..               | ..  | 6         |
| 3C 380*       | 0.692  | 7.1               | 1.8                | 13              | 44.68                                       | ..             | 13         | 57               | ..  | 2         |
| 1928+738*     | 0.302  | 4.4               | 2.6                | 11              | 43.21                                       | 0.7±0.7        | 6          | 105              | 10  | 6         |
| 3C403*        | 0.059  | 1.13              | 45                 | 51              | 41.48                                       | 0.7±0.4        | ..         | ..               | ..  | 19        |
| PKS 2101-490  | (1.04) | 8.1               | 6                  | 49              | 44.17                                       | ..             | 25         | 116              | ..  | 2         |
| PKS 2152-69   | 0.0283 | 0.56              | 10                 | 5.6             | 40.66                                       | 1.6±0.4        | ..         | ..               | ..  | 20        |
| 3C 454.3*     | 0.859  | 7.7               | 5.2                | 40              | 44.62                                       | ..             | 18         | 129              | ..  | 2         |

Notes

The scale is given in units of kpc per arcsec.

All sources are classified as quasars except for the 4 FR II radio galaxies: Pictor A, 3C219, 3C403, and PKS2152-69.

A “\*” after the source name indicates that an optical detection has been reported see <http://home.fnal.gov/~jester/optjets/>.

The redshift for PKS 2101-490 is uncertain (described as ‘tentative’ by Marshall et al. (2005)).

PKS2152-69 is odd, having a bright knot close to the core, and a disparity between the radio, optical, and X-ray distributions. Ly, De Young & Bechtold (2005) argue for a thermal interpretation of the X-ray emission.

## References

1, Fabian, Celotti & Johnstone (2003); 2, Marshall et al. (2005); 3, Schwartz et al. (2006); 4, Wilson, Young & Shopbell (2001); 5, Hardcastle & Croston (2005); 6, Sambruna et al. (2004); 7, Chartas et al. (2000); 8, Schwartz et al. (2000); 9, Siemiginowska et al. (2003); 10, Jorstad & Marscher (2004); 11, Aldcroft et al. (2003); 12, Comastri et al. (2003); 13, Chartas et al. (2002); 14, Siemiginowska et al. (2002); 15, Marshall et al. (2001); 16, Sambruna et al. (2001); 17, Kataoka et al. (2003); 18, Cheung (2004); 19, Kraft et al. (2005); 20, Ly, De Young & Bechtold (2005); 21, Siemiginowska et al. (2003).

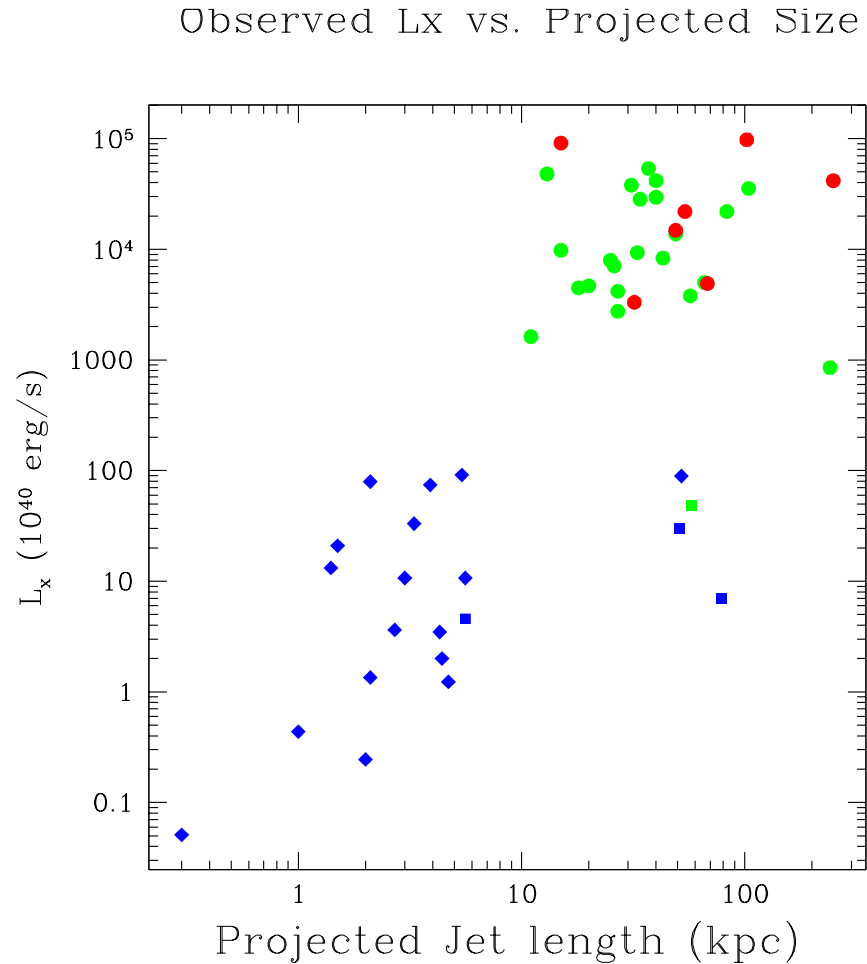


Figure 7: The observed X-ray luminosity plotted against the projected length of the jet. Quasars are plotted with filled circles; FRII radio galaxies with squares; and FRI radio galaxies (including Seyferts and BL Lac objects) with diamonds. The colors are allocated according to: red,  $z > 1$ ; green,  $1 > z > 0.1$ ; and blue,  $0.1 > z$ . The FRI (diamond) close to the 3 FRII's is 3C120 which has a weak detection of a knot  $80''$  from the nucleus. The FRII (square) jet in the midst of the main clump of FRI's is PKS2152-69. Ly, De Young & Bechtold (2005) present evidence that the X-ray emission of the jet related feature is thermal in origin.

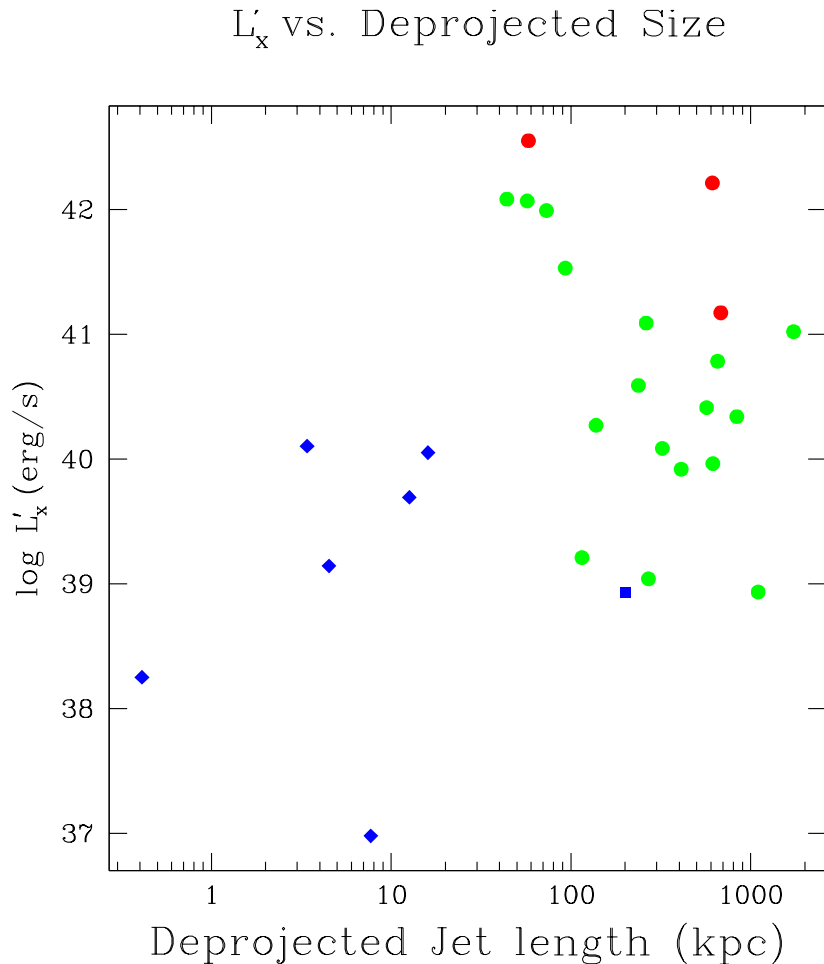


Figure 8: The best guess jet-frame luminosity corresponding to the observed X-ray luminosity, ( $L'_x=L_x(\text{obs})/\delta^4$ ), plotted against the deprojected length of the jet. The symbols are used the same way as in fig. 7.

Figure 9: The first part of the jet in 3C273. The quasar itself is well off this picture, up and to the left. The false color image is from a VLA map at 22 GHz, kindly supplied by R. Perley. The radio beamsize is  $0.35''$  FWHM. The color scale is below the image and given in Jy/beam. The contours are from recent CXO data, smoothed with a Gaussian of FWHM= $0.25''$ . The lowest contour is  $0.008 \text{ eV s}^{-1}$  per  $0.049''$  pixel and successive contours increase by factors of  $\sqrt{2}$ . Note how the radio ridge line heads directly south right after knot A; thus knot B1 lies on the northern edge of the jet in the UV and X-ray, but on the southern side of the jet in the radio. Although B1 and B2 are not well resolved with the CXO data, they are clearly separate in the radio and HST images (Jester et al. 2005).

Figure 10: The jet in Cen A. The colors show the X-ray image smoothed with an  $0.5''$  FWHM Gaussian and the contours are from the VLA at 8 GHz with a beamsize of  $1.1'' \times 0.25''$  (PA of major axis  $\approx 0^\circ$ ). The first contour level is 0.12 mJy/beam and successive intervals increase by factors of 4. This figure was provided by M. Hardcastle.

Figure 11: The jet of PKS1127-145. The colors show a Chandra X-ray image smoothed with an  $0.5''$  FWHM Gaussian and the contours are from the VLA at 8 GHz with a beamsize of  $0.78'' \times 0.58''$  in PA= $62^\circ$ . The first contour level is 0.2 mJy/beam and successive intervals increase by factors of  $\sqrt{2}$ . These new data will be published by Siemiginowska et al. (2006, in preparation).

\*

Figure 12: Profiles along the jet in 3C273. The quasar is off the plots to the left. The length shown is  $16.7''$  and the width used was  $2''$ . Top panel: the X-ray data smoothed with a Gaussian of FWHM= $0.25''$ . Middle: a profile from an archival HST exposure (F622W), smoothed with a Gaussian of  $0.5''$ . Bottom: a profile from an 8 GHz VLA map kindly supplied by R. Perley. The clean beam is  $0.5''$ . The vertical scales are linear, in arbitrary units.



This figure "fig01.jpg" is available in "jpg" format from:

<http://arxiv.org/ps/astro-ph/0607228v1>

This figure "fig02.jpg" is available in "jpg" format from:

<http://arxiv.org/ps/astro-ph/0607228v1>

This figure "fig03.jpg" is available in "jpg" format from:

<http://arxiv.org/ps/astro-ph/0607228v1>

This figure "fig06.jpg" is available in "jpg" format from:

<http://arxiv.org/ps/astro-ph/0607228v1>

This figure "fig09.jpg" is available in "jpg" format from:

<http://arxiv.org/ps/astro-ph/0607228v1>



This figure "fig10.jpg" is available in "jpg" format from:

<http://arxiv.org/ps/astro-ph/0607228v1>

This figure "fig11.jpg" is available in "jpg" format from:

<http://arxiv.org/ps/astro-ph/0607228v1>

This figure "fig12.jpg" is available in "jpg" format from:

<http://arxiv.org/ps/astro-ph/0607228v1>